UNIVERSIDAD DE CONCEPCIÓN
FACULTAD DE CIENCIAS FÍSICAS Y MATEMÁTICAS

Efectos del cambio climático en el hábitat marino del Pacífico sudoriental: Evaluación de múltiples estresores oceánicos a través de velocidades climáticas

Por: Leonardo Yévenes Vega

Tesis presentada a la Facultad de Ciencias Físicas y Matemáticas de la Universidad de Concepción para optar al grado de Magíster en Geofísica

Junio 2025
Concepción, Chile

Profesora Guía: Dra. Carolina Parada Veliz
Profesor Co-Guía: Dr. Boris Dewitte
Comisión Evaluadora: Dr. Javier Porobic, Dr. Héctor Sepúlveda Allende, Dra. Véra Oerder-Gautron

Universidad de Concepción
Facultad de Ciencias Físicas y Matemáticas
Departamento de Geofísica

Efectos del cambio climático en el hábitat marino del Pacífico sudoriental: Evaluación de múltiples estresores oceánicos a través de velocidades climáticas

Leonardo Yévenes Vega

Tesis presentada a la Facultad de Ciencias Físicas y Matemáticas de la Universidad de Concepción para optar al grado de Magíster en Geofísica

Profesora Guía: Dra. Carolina Parada Veliz
Profesor Co-Guía: Dr. Boris Dewitte
Comisión Evaluadora: Dr. Javier Porobic, Dr. Héctor Sepúlveda Allende, Dra. Véra Oerder-Gautron

Junio 2025, Concepción, Chile

A Flor, Cheo y Máximo

AGRADECIMIENTOS

En primer lugar, agradezco a mi familia, quienes siempre han estado, listos para festejar cada logro, sin importar lo pequeño que sea. En especial agradezco a mi padre Cheito, por enseñarme a no rendirme, y que todo se consigue con esfuerzo y perseverancia, a mi madre Flor por enseñarme que no existe problema sin solución, no importa que tan terrible parezca, y a Máximo mi mascota, que me enseñó a sonreír, agradecer y disfrutar la vida, hasta en los días más grises. Todo esto es por y para ustedes.

Agradezco el invaluable apoyo de mis hermanos de la vida, Cesar, Andrés, Barbara, Seba, Pacha, Mati, Horma, Vale y Mauro, quienes en momentos de duda me aconsejaron, en la frustración me escucharon y en la debilidad nunca me dejaron decaer, recordándome quien soy y de lo que soy capaz. Espero nunca esperen menos de mí. Agradezco la compañía y soporte incondicional que me ha brindado mi pareja Antonia, quien ha llevado el peso de mantener un hogar, mientras yo pasaba los días trabajando, quien me ayudo a levantarme, cuando no tenía energías, y quien me recordó descansar cuando más lo necesitaba, pero olvidaba hacerlo. Este logro es de ambos.

Agradezco a Caly, la mejor guía. Gracias por enseñarme a abrir y flexibilizar la mente, a entender que no se trata de lo que creemos, sino de lo que descubrimos, a no tener miedo a lo que se viene, sin importar de dónde venimos, a aceptar y agradecer, aunque no sea lo que queremos o esperamos, que no importa que tan largo y duro sea camino, porque con esfuerzo y persistencia siempre llegarás al final, y sobre todo te agradezco por creer siempre en mí, incluso cuando yo no podía. Espero algún día poder guiar como tú, el mundo lo necesita. Agradezco al Programa de Magíster en Geofísica y al Departamento de Geofísica de la UDEC, por permitirme desarrollar este trabajo. Al proyecto CLAP del CEAZA, a Billy y Caly por su apoyo financiero, el cual ha sido clave durante estos años.

Finalmente agradezco a la enorme lista de personas que, de una u otra forma, me ayudaron y apoyaron en esta etapa. Hacer ciencias es complejo, es un camino lleno de obstáculos y callejones sin salida, una tarea imposible sin el apoyo que nos entregamos unos a otros, sin colaboración no hay ciencia, y sin ustedes, este trabajo no sería posible. Por todo esto ¡muchas gracias!

Resumen

El cambio climático constituye un fenómeno de creciente relevancia en la agenda global, tanto por la complejidad de sus causas—entre las que destacan la fuerte dependencia de la sociedad moderna de los combustibles fósiles y las actividades de uso del suelo—como por la magnitud de sus efectos a largo plazo, los cuales modifican de manera significativa los procesos naturales en los ámbitos físicos, químicos y biológicos. El Océano es altamente afectado por este fenómeno, provocando a escala global calentamiento, desoxigenación y reducción de pH, los cuales de manera individual y conjunta inducen cambios importantes en los ecosistemas marinos. A pesar de la gravedad de esto, la información sobre sus efectos a escalas regionales es escasa, como es el caso del océano Pacífico sudoriental, una región que presenta zonas de alto endemismo, biodiversidad marina y productividad pesquera. Su altísima importancia biológica y económica hacen imperante el avance en estudios sobre los efectos nocivos específicos del cambio climático en esta región.

En este trabajo estudiamos los efectos del cambio climático en el océano Pacífico sudoriental, a través del cálculo de la velocidad climática, para la temperatura, oxígeno y pH. Esta herramienta, ampliamente usada y recomendada, nos permite segmentar una región según su estado de conservación, migración o pérdida climática. A través de un enfoque multidimensional, evaluamos y comparamos dos periodos (2015–2050 contra 2015–2100) y tres profundidades de la capa epipelágica (0, 100 y 200 m), bajo dos escenarios climáticos, que contemplan un futuro basado en el uso de combustibles fósiles (SSP5-8.5), o un futuro sustentable (SSP1-2.6). Además, estudiamos cinco casos de zonas particulares, tres comprenden archipiélagos e islas, con alto endemismo y biodiversidad, y dos corresponden a sistemas de surgencia de alta productividad e importancia económica.

Se identificó que, bajo un escenario futuro caracterizado por un alto uso de combustibles fósiles (SSP5-8.5, periodo 2015–2050), predominan las áreas sujetas a migración y pérdida de condiciones climáticas regulares de las variables analizadas; sin embargo, también se reconocen múltiples zonas que podrían funcionar como refugios climáticos. Tres refugios climáticos de temperatura: dos en los trópicos (uno en 5°S a 100 m de profundidad, y otro en 10°S a 200 m de profundidad), y uno al sur de Chile (55°S desde 0 a 200 m de profundidad), y un refugio climático de oxígeno subsuperficial (100 y 200 m) en gran parte del ecuador (desde 10°S a 10°N)

y del Gran Ecosistema Marino de la Corriente de Humboldt (HCLME). El último sector también presenta las velocidades climáticas más bajas de reducción de pH (es decir, zonas de cambio climático lento), resaltando su importancia como zona clave para la conservación marina. Por otro lado, al comparar las zonas de enfoque, se sugiere que la zona más afectada es Rapa Nui, seguido de los archipiélagos en el extremo oeste del HCLME, y finalmente las zonas de surgencia costera, proponiendo que las zonas más alejadas en el océano son más proclives ante el cambio climático. Finalmente, se observó que las condiciones de temperatura y pH experimentarán una menor variación bajo un escenario de mitigación, con una tendencia decreciente a lo largo del tiempo; en contraste, dichas condiciones se verían agravadas en un escenario futuro basado en un elevado uso de combustibles fósiles.

Índice general

Índice de cuadros

Índice de figuras

Capítulo 1

1.1. Introducción

El cambio climático (CC), impulsado por las emisiones de carbono procedentes de los combustibles fósiles y las actividades de cambio de uso del suelo [1-3] conlleva amenazas significativas para los ecosistemas marinos [4-6], al forzar cambios biogeoquímicos oceánicos como la desoxigenación, el calentamiento y la reducción de pH en los océanos [3, 7-10]. Si bien estos efectos han sido bien documentados a escala mundial, no necesariamente se replicarán en escalas locales, donde operan dinámicas particulares de los ecosistemas y la biodiversidad marina. Esto aplica al océano Pacífico Sudoriental (SEP), una zona con regiones biogeográficas contrastantes, alta biodiversidad y endemismo marinos [11-14], asociada a gradientes marcados en las propiedades del agua, debido una surgencia costera permanente y a la presencia de una zona de mínimo oxígeno (OMZ). Dentro del SEP se encuentra el Gran Ecosistema Marino de la Corriente de Humboldt (HCLME), una de las zonas más productivas del mundo caracterizada por una gran diversidad de especies y la mayor actividad pesquera de los cuatro sistemas de surgencia de límite oriental [9, 15-17]. En los últimos 15 años, se han creado diversas Áreas Marinas Protegidas (LSMPAs) dentro del SEP, que albergan ecosistemas vulnerables, que comprenden islas oceánicas y montes submarinos, como es el caso del Archipiélago Juan Fernández (JFA), Archipiélago Desventuradas (DA) y Rapa Nui (RN) [18]. Dichos sistemas están conectados de algún modo, gracias a la circulación del giro anticiclónico de gran escala, caracterizada por un flujo dominante desde JFA hacia DA, que se curva hacia el oeste en dirección a RN [14, 19, 20]. Se ha documentado conectividad entre los archipiélagos [21, 22], los sistemas de montes submarinos y la costa occidental de Sudamérica [23].

En el contexto del CC, se espera una elevada presión sobre las especies marinas, lo que puede desencadenar migraciones, dependiendo de la tolerancia y capacidades adaptativas de las especies [24, 25, 12]. Sin embargo, esos impactos son difíciles de evaluar, debido a la escasez de datos sobre los rasgos fisiológicos de las especies que habitan el SEP [26], sumado al hecho que los modelos climáticos globales, que constituyen la base de la mayoría de los estudios de impacto, están cargados de incertidumbres [27]. No obstante, hay algunos efectos del CC que han sido bien documentados. Con respecto a la temperatura superficial del mar, el patrón de CC en el SEP es similar a El Niño, caracterizado por una tasa de calentamiento fuerte, que se extiende desde el Pacífico ecuatorial hasta la costa de Perú y el norte de Chile, y una tasa de calentamiento mucho más débil en los subtrópicos de mar abierto [20]. Este patrón se asocia al debilitamiento de los vientos alisios [28, 29], mientras que la tasa relativa de calentamiento mínimo en los subtrópicos se asocia a cambios en la circulación atmosférica de bajo nivel, inducidos por la expansión de la celda de Hadley [30-33]. Si bien existe un amplio consenso entre los modelos en cuanto al patrón general de calentamiento, estos discrepan en la intensidad de la taza de calentamiento y la forma en que este penetra en la subtermoclina [34]. En cuanto a los patrones de oxígeno en el SEP, existe incertidumbre sobre el comportamiento futuro del límite superior de la OMZ. Mientras que la mayor parte del océano SEP se desoxigenará como consecuencia del calentamiento [35, 36], las proyecciones globales de los Earth System Models (EMSs) indican que es más probable que se erosione el límite superior de la OMZ [37], favoreciendo teóricamente la expansión del hábitat epipelágico [26]. Fuera de la OMZ, la desoxigenación puede afectar a las especies costeras (por ejemplo, Grimothea monodon, ex Pleurocondes monodon [38]) y vulnerables de los sistemas insulares (en función de su tolerancia). Por otra parte, se prevé que el pH global se reduzca debido al CC [7, 24, 39-41], lo que, acoplado al calentamiento y la desoxigenación, puede crear presiones compuestas sobre los hábitats marinos y perturbar redes tróficas marinas enteras.

Comprender cómo los factores múltiples estrés se propagan en cascada a través de las redes tróficas o alteran los servicios ecosistémicos es un reto, debido tanto a la complejidad de las interacciones entre estos factores de estrés y sus efectos en los ecosistemas marinos. Las estrategias de conservación y gestión suelen abordar factores de estrés individuales (por ejemplo, áreas marinas protegidas definidas por calentamiento o gestión de nutrientes para la desoxigenación), en lugar de sus efectos

combinados. En este trabajo, reconociendo la complejidad de este reto, pretendemos profundizar nuestra comprensión sobre cómo los patrones de CC descritos previamente afectan teóricamente a los hábitats marina. Herramientas como la "velocidad climática" se han denominado fundamentales para resolver las brechas de conocimiento sobre los efectos del CC en los ecosistemas marinos. La velocidad climática, definida como la velocidad y dirección a la que cambian los climas, y los caminos que podrían seguir las especies para mantener sus condiciones preferidas [42], proporciona un enfoque valioso para comprender los cambios en los hábitats, en respuesta a la alteración de variables oceánicas como la temperatura, el oxígeno y el pH [43]. Numerosos estudios han utilizado la velocidad climática para evaluar posibles hábitats futuros en diferentes ecosistemas [5, 20, 26, 44-47]. Más aún, la velocidad climática se ha propuesto como una herramienta útil para determinar refugios climáticos, definidos por [48] como regiones con retención climática de largo plazo, lo que les confiere un gran valor de conservación y permite a las especies sobrellevar los efectos negativos del CC en el futuro [5, 47-52]. Nuestro enfoque implica estimar velocidades climáticas [5, 42, 46] de temperatura, oxígeno y pH, lo que nos permitió detectar regiones de refugio y exposición climática, para todo el SEP y para cinco zonas específicas dentro de este, compuestas por islas de ecosistemas altamente vulnerables (JFA, DA y RN) y zonas de surgencia de alta relevancia económica, como el Sistema de Surgencias del Norte de Chile (NCU; 18°-30°S), y el Sistema de Surgencia del Centro-Sur de Chile (SCCU; 32°-41°S) (figura 1), para explorar los cambios tanto en alta mar como en tierra.

1.2. Propósito de la tesis

1.2.1. Formulación del problema

El SEP es una región altamente relevante, tanto ecológica como económicamente, debido a su elevada biodiversidad, alto nivel de endemismo y gran productividad primaria, capaz de sostener actividades pesqueras de gran escala. Sin embargo, esta zona enfrenta crecientes amenazas asociadas al cambio climático, el cual a escala global induce el aumento de la temperatura, la disminución del oxígeno y la acidificación del océano (reducción del pH). Estos tres factores alteran de forma directa las condiciones que definen los hábitats marinos, comprometiendo su estabilidad y resiliencia.

A pesar del alto riesgo que representan estos cambios en los ecosistemas marinos,

la comprensión de sus impactos en el SEP sigue siendo muy escasa, limitando la capacidad de anticipar cambios ecosistémicos, identificar zonas vulnerables o resilientes, o diseñar medidas efectivas de conservación y manejo pesquero. Frente a este escenario, surge la necesidad de evaluar qué zonas del SEP serán más o menos afectadas por el cambio climático, estudiando posibles cambios en variables clave como la temperatura, el oxígeno y el pH.

En este estudio se aborda este problema, a través del uso de las velocidades climáticas. Se busca diferenciar zonas dentro del SEP, según su estado de cambio climático, para tres profundidades de la capa epipelágica, comparando dos escenarios contrastantes, tanto a un futuro cercano, como lejano. El análisis de la velocidad climática, aplicado sobre proyecciones del CMIP6, ofrece una herramienta adecuada para identificar zonas de conservación, migración o pérdida climática, y así aportar evidencia científica relevante para guiar estrategias de adaptación y conservación. Este estudio, por tanto, se enfoca en cuantificar estos patrones bajo dos escenarios contrastantes (SSP5-8.5 y SSP1-2.6), vinculados a posibles trayectorias futuras de desarrollo social, económico y ambiental, con el objetivo de mejorar nuestra comprensión del cambio climático en el SEP, identificar áreas prioritarias y caracterizar las dinámicas particulares de zonas biológica y económicamente relevantes.

1.2.2. Objetivos de investigación

En este estudio buscamos evaluar el efecto del cambio climático en los ecosistemas epipelágicos del Océano Pacífico sudoriental, a través del cálculo de las velocidades climáticas sobre tres factores que determinan las condiciones particulares de cada hábitat marino: temperatura, oxígeno y pH.

1.2.2.1. Objetivos específicos

1. Determinar horizontalmente zonas de conservación, migración y pérdida climática, para las tres variables mencionadas, en tres profundidades equidistantes dentro de la capa epipelágica (0, 100 y 200 m), y así sugerir qué zonas presentan mayor o menor resistencia al cambio climático.

2. Estimar las zonas más propensas al cambio climático, definidas como áreas que pertenezcan al 25 % de las velocidades climáticas más rápidas.

3. Evaluar las diferencias en los patrones espaciales de estas áreas (objetivo 2),

bajo escenarios climáticos contrastantes (uno basado en el uso intensivo de combustibles fósiles y otro en un desarrollo sustentable), con el fin de explorar la variabilidad de impactos potenciales tanto a corto (2015–2050) como a largo plazo (2015–2100).

4. Estudiar y comparar los efectos del cambio climático en zonas específicas (archipiélago de Juan Fernández, Archipiélago Desventuradas, Rapa Nui, zona de surgencia del norte de Chile y la zona de surgencia centro-sur de Chile), elegidas por su destacada importancia biológica y económica, buscando patrones de similitud o diferencias, en sistemas con dinámicas particulares.

1.2.2.2. Hipótesis de investigación

Hipótesis: Los cambios inducidos por cambio climático son altamente complejos, debido a las dinámicas físico-químicas individuales y sinérgicas entre las variables oceánicas de interés (en nuestro caso temperatura, ph y oxígeno), que cambian tanto vertical como horizontalmente. Por lo anterior, hipotetizamos que:

Ho1: Se plantea que, en el SEP, existen zonas altamente vulnerables al cambio climático (pérdida climática), así como áreas que podrían mostrar resistencia (bajas velocidades climáticas) o mantenerse inalteradas (conservación climática). Estas diferencias en las zonas identificadas son independientes de las variables consideradas, como la profundidad o el tipo de factor climático evaluado, sugiriendo que su comportamiento no depende exclusivamente de una sola variable.

Ho2: se postula que el escenario climático sustentable presenta menores velocidades climáticas en todas las variables analizadas en comparación con el escenario de uso de combustibles fósiles, independientemente del periodo (corto o largo plazo) considerado en el estudio.

Hipótesis Alternativa:

H1: A pesar de la complejidad de las dinámicas oceánicas, la influencia del cambio climático es constante y general, generando patrones estables influidos principalmente por el calentamiento.

H2: El escenario climático sustentable, en comparación con el escenario basado en el uso de combustibles fósiles, no presenta menores velocidades climáticas en todos los casos, para todas las variables.

Capítulo 2

Effects of climate change on marine habitat in the southeastern Pacific: Multiple ocean stressors assessed through climate velocities

2.1. Abstract

Anthropogenic climate change has triggered a cascade of impacts on marine ecosystems, often referred to as the "deadly trio": warming, acidification, and deoxygenation. While these stressors will globally lead to the compression of marine habitats, their regional effects vary significantly and remain understudied. This is particularly true for the southeastern Pacific (SEP), which supports rich pelagic and benthic ecosystems closely linked to a complex seafloor featuring archipelagos and extensive seamount chains. Using model simulations from Phase 6 of the Coupled Model Intercomparison Project (CMIP6), this study examines future regional-scale environmental changes in the SEP. Our analysis builds on the observation that the South Pacific Ocean Gyre is among the regions experiencing the least warming globally and that the epipelagic zone within the oxygen minimum zone may oxygenate in the future. These conditions may promote habitat expansion, which we assess using the climate velocities for temperature, oxygen, and pH. We demonstrate that, in a pessimistic near future (2015–2050), most regions show a potential climatic loss in the entire epipelagic layer. However, two broad areas benefit from conservation below the surface: a region in the tropics extending from 10°S – 100°W to the east of Rapa Nui and the coastal region of Peru and Chile, extending up to the Desventuradas and Juan Fernández archipelagos. While the former is due to the slow warming rates,

the latter results from both slow deoxygenation and oxygenation climate velocities along the coast of those countries, a zone that overlaps with the lowest changes in pH in the SEP, giving them a unique conservation value. We demonstrate that epipelagic ecosystems within the oxygen minimum zone may be less impacted by climate change than those outside of it.

2.2. Introduction

Climate change (CC), driven by carbon emissions from fossil fuels and land-use change activities [1-3], is reshaping ocean biogeochemistry and threatening marine ecosystems [4-6], by forcing ocean biogeochemical changes such as ocean deoxygenation, warming, and pH reduction [3, 7-10]. Although those effects have been well documented on a global scale, we cannot assume that smaller-scale locations, which support specific ecosystem dynamics and marine biodiversity, will experience the same effects. This applies to the southeastern Pacific (SEP), a region with contrasted biogeographical regions and a high marine biodiversity and endemism [11-14], associated with a marked mean gradient in water properties because of the permanent coastal upwelling and an oxygen minimum zone (OMZ). The SEP encompasses the Humboldt Current Large Marine Ecosystem (HCLME), one of the most productive zones in the world characterized by a high species diversity and the highest fishing activity of the four eastern boundary upwelling systems [9, 15-17]. Several large-scale marine protected areas (LSMPAs) have been created within the SEP over the past 16 years. These areas host vulnerable ecosystems, such as oceanic islands and seamounts, as is the case of the Juan Fernandez Archipelago (JFA), Desventuradas Archipelago (DA), and Rapa Nui (RN) [18]. Such systems are somehow connected because of the large-scale anticyclonic gyre circulation, characterized by a dominant flow from JFA towards DA, which bends westwards towards RN [14, 19, 20]. Connectivity between the archipelagos [21, 22], seamounts systems and the west coast of South America [23] have been documented.

Global warming is expected to result in high pressure on marine species, which may trigger migration, depending on the species' tolerance and adaptive capacities [12, 24, 25]. However, such impacts are difficult to assess because data on the physiological traits of species inhabiting the SEP are scarce [26] and because global climate models, which form the basis of most impact studies, are burdened with uncertainties [27].

Nevertheless, some CC effects have been well documented. In terms of sea surface temperature, the CC pattern in the SEP is El Niño-like, characterized by a stronger warming rate extending from the equatorial Pacific to the coast of Peru and northern Chile and a much weaker warming rate in the open-ocean subtropics [20] The El Niño-like pattern is associated with the weakening of trade winds [28, 29]. On the other hand, the relative minimum warming rate in the subtropics is associated with changes in the low-level atmospheric circulation induced by the expansion of the Hadley cell [30-33]. Although the models largely agree on the overall pattern, they vary significantly in the magnitude of the warming rate and its penetration into the sub-thermocline [34]. The uncertainty regarding oxygen trends in the SEP concerns the future behavior of the upper bound of the OMZ. While most of the SEP will deoxygenate due to warming [35, 36], projections from global Earth System Models (EMSs) suggest that the upper bound of the OMZ is more likely to be eroded [37], theoretically favoring the expansion of epipelagic habitats [26]. Outside the OMZ, deoxygenation may impact coastal (e.g. *Grimothea monodon*, ex *Pleurocondes monodon*, [38]) and vulnerable species of the island systems. In addition, the global oceanic pH is projected to decrease because of CC [7, 24, 39-41], which, coupled with warming and deoxygenation, can create compounding pressures on marine habitats and disrupt entire marine food webs.

Understanding how cumulative stressors cascade through food webs or disrupt ecosystem services is challenging because of the complex interactions among these factors and their effects on marine ecosystems. Conservation and management strategies often focus on individual stressors such as marine protected areas for warming or nutrient management for deoxygenation, rather than their compounded effects. Here, recognizing the complexity of this challenge, we aim to deepen our understanding of how the previously described patterns of CC impact theoretical marine habitability. Climate velocity has emerged as critical for addressing knowledge gaps about the effects of CC on marine ecosystems. Climate velocity, defined as the speed and direction at which climates shift and the paths species may follow to maintain their preferred conditions [42], provides a valuable framework for understanding habitat changes in response to altered ocean variables such as temperature, oxygen, and pH [43]. Several studies have used climate velocity to assess future habitats across different ecosystems [5, 20, 26, 44-47]. Furthermore, climate velocity has been proposed as an useful tool to determine climate refugia,

defined by [48] as regions with long-term climate retention, which gives them high conservation value and enables species to withstand the negative effects of CC in the future [5, 47-52]. Our approach involves estimating the climate velocities [5, 42, 46] of temperature, oxygen, and pH, enabling us to map regions of climatic refugia and exposure, for the entire SEP and five specific zones within it. These zones, include highly vulnerable island ecosystem (JFA, DA, and RN) and upwelling zones with high economic relevance, such as the Northern Chilean Upwelling System (NCU, 18°–30°S) and the Southern-Central Chilean Upwelling System (SCCU, 32°–41°S) (Figure 2.3.1), to explore both offshore and onshore changes.

2.3. Methodology

2.3.1. Earth System Models for the southeastern Pacific

The ESMs used in this study belong to Phase 6 of the Coupled Model Intercomparison Project (CMIP6, [53]) under two contrasting scenarios: 1) The SSP1-2.6 scenario (Sustainability) and 2) the SSP5-8.5 scenario (Fossil-fueled Development) (see Section 2.7.1.1 or [54] for the scenarios' details). Seventeen models were used for temperature, 11 for oxygen and 10 for pH (see Tables 2.9.1 and 2.9.2). Model selection was constrained by data availability rather than a systematic criterion. However, by focusing on the ensemble mean for each variable, we assume that these subsets provide an overall average that minimizes the uncertainty associated with the structural model error [27]. Model variables were bilinearly interpolated on a common $1° \times 1°$ horizonal grid. Vertically, we select three depths within the epipelagic layer (surface, 100, and 200 m). Monthly means for 2015–2100 were used.

We focus on the SEP (defined as 0°–60°S and 70°–130°W) and five zones within it (Figure 2.3.1). Three of these zones were located around islands (200 nm around the center) and two were eastern boundary upwelling systems (200 nm from the coast). The island zones [13, 20] corresponded to JFA (33.64°S, 78.84°W), DA (26.32°S, 80°W) and RN (27.12°S, 109.35°W), and the upwelling systems corresponded to the NCU (18°–30°S, 70°–71.5°W), with constant favorable upwelling winds all year round, and the SCCU (35°–41°S, 72°–73.5°W), with highly seasonal favorable upwelling winds [55].

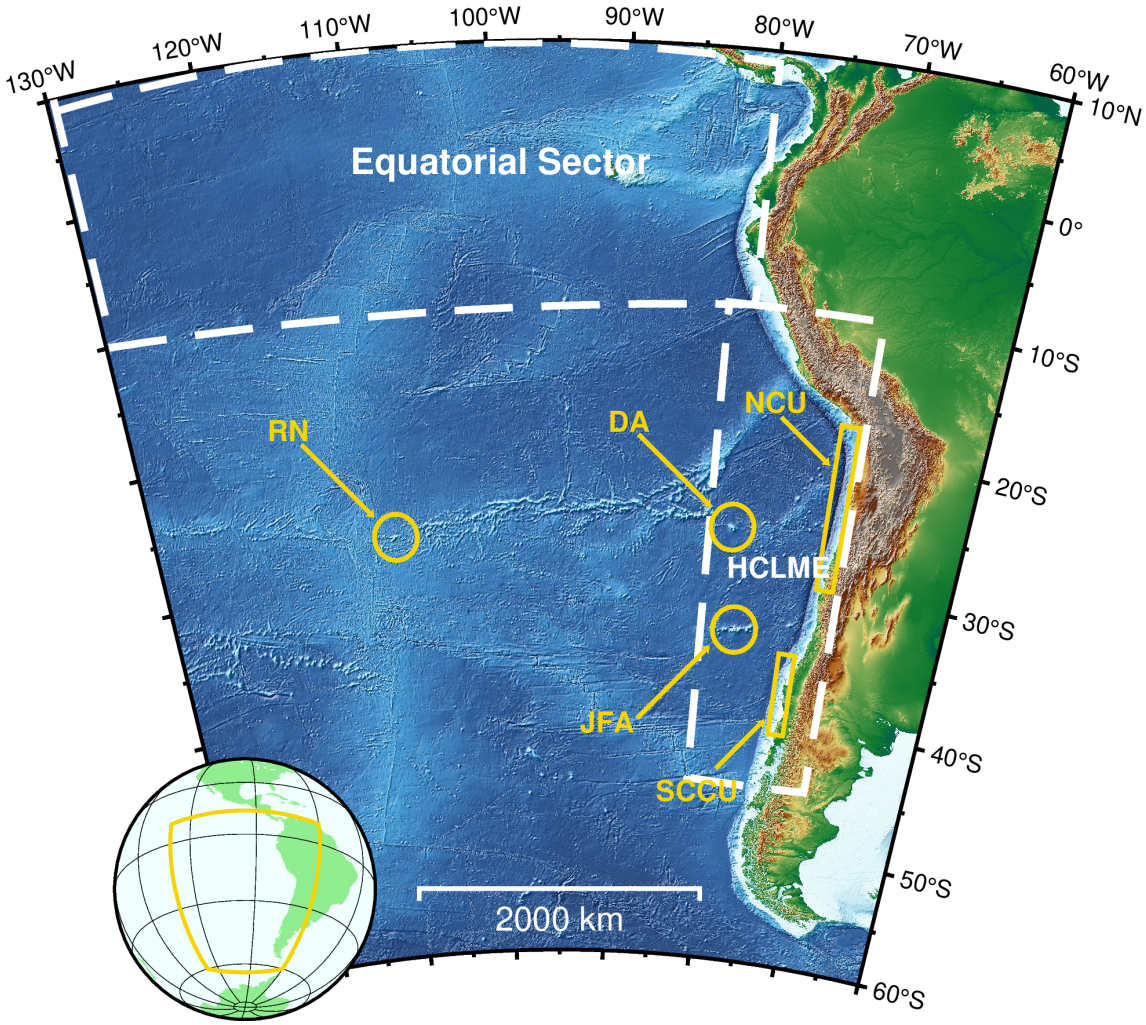

Figure 2.3.1: Map of the domain and focal zones. The study area extends over the domain 130° to 60°W and 10°N to 60°S. The focal zones of study are Rapa Nui (RN), Desventuradas Archipelago (DA), Juan Fernandez Archipelago (JFA), Northern Chilean Upwelling System (NCU), and the Southern-Central Chilean Upwelling System (SCCU).

2.3.2. Climate velocity

Climate velocity, which corresponds to the rate at which the average conditions of a variable (hereafter defined as climate) move (shift, expand, or contract) in kilometers per year ($\frac{km}{yr}$) was estimated. The climate velocity corresponds to the ratio between a temporal trend (e.g. $s = \frac{^\circ C}{yr}$) and a spatial gradient ($g = \frac{^\circ C}{km}$) [42], and was calculated following [46], using the VoCC package in R [56]. We used the gradient-based approach ($gVoCC = \frac{s}{g}$) where the time trend (s) is estimated as the slope of the linear regression of the time series of a focal cell, and the two-dimensional

spatial gradient (g), calculated on a 3×3 grid (around the focal cell) [44]. The climate velocity was estimated for temperature, oxygen, and pH at the three selected depths (surface, 100, and 200 m) and for two periods (2015–2050, 2015–2100) to evaluate changes between near and far future. The climate velocities for the second period (2015–2100) were used for the calculation of the fastest zones (FZ) (see Methodology Section 2.4). The ensemble means of the variables were obtained before the climate velocity was calculated. The associated error of the estimation was assessed using a bootstrap method [57], which involved calculating the climate velocity of 1000 random samples from the models' ensemble. Each bootstrap sample represents the average of a random selection with replacement of the 17, 11, and 10 models for temperature, oxygen, and pH, respectively. The spatial gradient threshold, which defines the minimum possible value of spatial gradient to be used in the climate velocity calculation, was set at 10^{-4} following [46]. There is no established method for defining this threshold in a multi-stressor context. Therefore, in this study we will apply the same value to all three variables. The supplementary material presents the results of sensitivity test for this threshold (see Section 2.7.1.2 and Figure 2.8.3). The conclusions of this paper are unaffected by the choice of threshold within the tested range.

2.3.3. Climate states: from conservation to loss

Climate velocity trajectories, corresponding to the path followed by a climate in a specific period were determined based on the methodology of [45], who split them into nine categories: non-moving, slow-moving, relative sink, coastal sink, internal sink, source, corridor, divergence and convergence (Table 2.9.6). These climatic categories are then classified into four primary climate states: conservation, migration, loss or oxygenation/cooling. Climate conservation corresponds to the cells where no significant climatic displacement occurred (displacement $<$100 km) in the total period (non-moving and slow-moving). Climate migration corresponds to the cells where a high climatic arrival or departure was observed (divergence and convergence). Climate loss corresponds to cells where climate disappears, or migrate excessively, with low residence time (sink, coastal sink, internal sink, source and corridor). Migration and loss classifications apply only to climate velocities of warming, deoxygenation and pH reduction climate velocities. Climate oxygenation/cooling classification applies to cells where climate velocities of oxygenation or cooling are fast enough to avoid being

classified as conservation zones. Additionally, we use the conservation classification to identify climate refugia, areas that retain their climates over long periods, allowing species to resist future harmful impact of CC and providing high conservation value [48]. We focused on the climate velocities (section 2.2) and climatic state (section 2.3) analysis of the "fossil-fueled" scenario in the near future to prioritize the outcomes of the worst possible case, which corresponds to the current global socioeconomic pathway. The supplementary material presents the results for the "sustainability" scenario (Figures 2.8.1 and 2.8.2).

2.3.4. Fastest climate velocity zones

The fastest climate velocity zones or fastest zones (FZ) are the areas most affected by individual or combined stressors. The temporal evolution of these zones was assessed by comparting far and near future periods to identify whether the zone expands, contracts, disappear, or new ones will emerge. The FZs calculation was based on climate velocity and represented 25 % of the highest climatic velocities for all the SEP for the near future. The FZ for temperature was defined as the zones where the climate velocities for this parameter are above the 75th percentile of the distribution corresponding to the whole SEP. By contrast, because the climate velocities associated with deoxygenation and acidification are negative, the FZs for oxygen and pH were defined as the zones where the corresponding climate velocities are below the 25th percentile for each scenario and depth (Table 2.3.1).

Table 2.3.1: Fastest zones thresholds ($\frac{km}{yr}$, with associated standard error estimate by bootstrap resampling $n = 1000$), calculated as the 25 % fastest climate velocities of the near future. These thresholds correspond to the 75th percentile of the climate velocity for temperature and the 25th percentile of the climate velocities for oxygen and for pH. * Indicates values less than twice the standard error.

	SSP5-8.5			**SSP1-2.6**		
Depth (m)	Temperature	Oxygen	pH	Temperature	Oxygen	pH
0	11.93 ± 0.99	-11.87 ± 0.92	-36.94 ± 0.41	4.37 ± 0.54	-7.72 ± 0.62	-18.3 ± 0.25
100	7.63 ± 0.47	-5.22 ± 0.59	-37.32 ± 4.14	4.45 ± 0.44	-8.05 ± 5.12*	-19.17 ± 1.87
200	9.86 ± 0.63	-5.4 ± 0.83	-36.1 ± 2.90	7.17 ± 0.68	-9.06 ± 6.94*	-20.66 ± 1.87

2.4. Results and discussion

2.4.1. Climate velocities and conservation state of the SEP

First, we analyzed the climate velocity patterns for each variable at the selected depths for the worst near-future case (the "fossil-fueled" scenario for 2015–2050, Figure 2.4.1). The highest warming climate velocities affected most of the Equatorial Sector (10°S to 10°N, Figure 2.3.1), following the El Niño-like pattern [58-60], across all depths (Figures 2.4.1(a), (b) and (c)). The HCLME (Figure 2.3.1) also presented high climate velocities at 100 and 200 m (Figures 2.4.1(b) and (c)), similar to [20]. This pattern was also found by [47], but from 2000 to 2019, suggesting that it has been maintained for a longer period. This could be due to the lack of surface-cooling mechanisms (like upwelling), which only affect the upper levels [47, 61, 62]. The Equatorial Sector and the HCLME at the subsurface are characterized as regions that experience climatic temperature loss (Figures 2.4.2(a), (b) and (c)). On the other hand, three temperature climate refugia were found: two in the tropical subsurface (5°S at 100 m, 10°S at 200 m) which extends eastward at least 40° from 130°W, despite the tropic's thermal expansion [63-65], and another one located in southern Chile (55°S) across all depths (Figures 2.4.2(a), (b) and (c)).

The climate velocities for oxygen and temperature at the surface were remarkably similar, with the highest deoxygenation velocity at the Equatorial Sector, showing mainly oxygen climatic loss (Figures 2.4.1(d) and 2.4.2(d)). This result is expected because oxygen concentrations are greatly influenced by surface heat. By contrast, the subsurface presents both slow deoxygenation and oxygenation climate velocities at the equatorial sector and the HCLME (Figures 2.4.1(e) and (f)), which are mostly classified as climate conservation regions, and therefore, oxygen climate refugia (Figures 2.4.2(e) and (f)). At depths of 100 and 200 m, the processes modeling the distribution and patterns of oxygen differ from those of warming. Indeed, vertical advection, OMZs, and subsurface currents are some of the major factors influencing the oxygen balance [66, 67]. These results support the negative climate velocity for oxygen (deoxygenation) in the HCLME surface (Figure 2.4.1(d)), but positive (oxygenation) at 100 m, which extends with increasing depth to 200 m (Figures 2.4.1(e) and (f)). This observation is consistent with [20] and [37], who explain the effect of oxycline deepening and OMZ erosion during El Niño events.

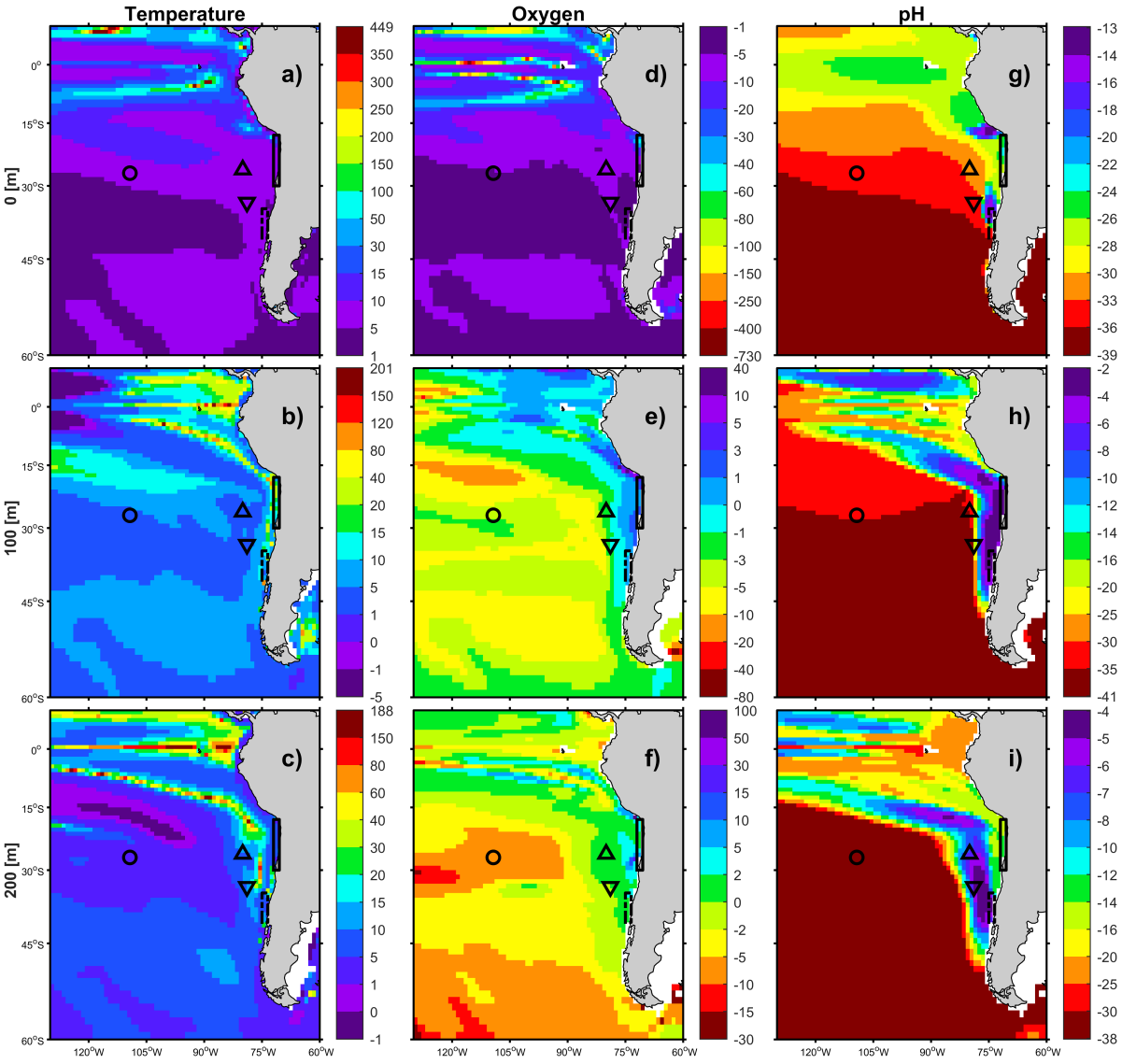

Figure 2.4.1: Climate velocities ($\frac{km}{yr}$) for the "fossil-fueled" scenario (SSP5-8.5) at near future: 2015–2050, for temperature at (a) 0 m, (b) 100 m, (c) 200 m, oxygen at (d) 0 m, (e) 100 m, (f) 200 m, and pH at (g) 0 m, (h) 100 m, (i) 200 m.

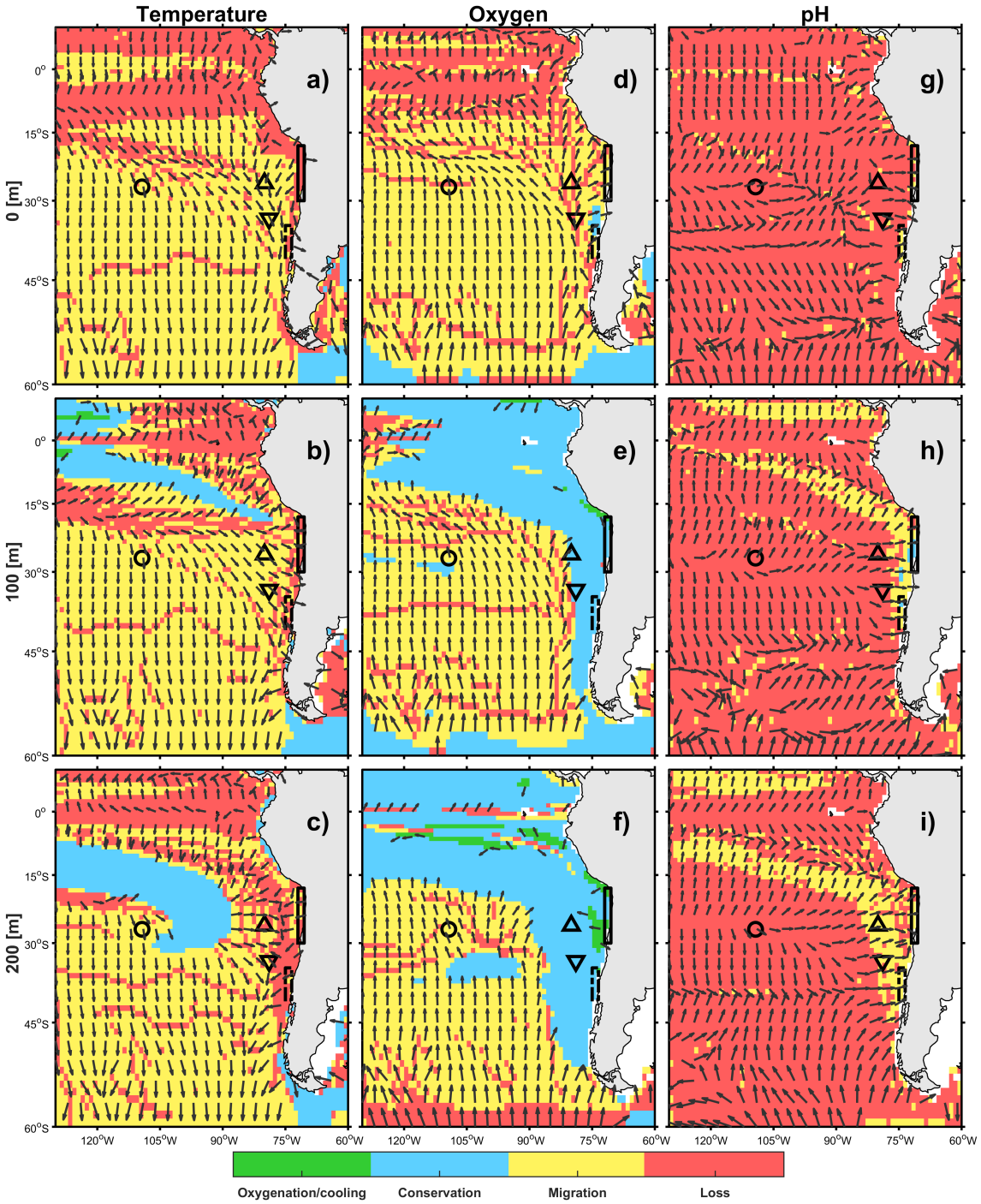

Figure 2.4.2: Climate state for the "fossil-fueled" scenario (SSP5-8.5) at near future: 2015–2050, for temperature at (a) 0 m, (b) 100 m, (c) 200 m, oxygen at (d) 0 m, (e) 100 m, (f) 200 m, and pH at (g) 0 m, (h) 100 m, (i) 200 m. The colors represent climate conservation (cyan), climate migration (yellow), climate loss (dark orange) and climate oxygenation/cooling (green).

All the SEP exhibits a climate velocity pattern of pH reduction (Figures 2.4.1(g),

(h) and (i)); thus, the SEP will experience a decline in pH, in every case, following the global ocean pH reduction trend [40], which is higher under high-emissions scenarios (SSP5-8.5) than under mitigation scenarios (SSP1-1.9, [41]). Nevertheless, the HCLME presents the slowest pH reduction climate velocity (slower at the subsurface than at the surface; Figures 2.4.1(g), (h) and (i)) and is the only region that presents more pH climate migration than loss, and even conservation (0,28 % at 100 m; Table 2.4.2, Figures 2.4.2(h) and (i)). This phenomenon may be due to the relatively high basal acidity of this zone [9] which could lead to slower changes. The pH presents the most homogeneous climate velocities among the variables (ranging from 10 to 30 $\frac{km}{yr}$), which may be due to the regional dampening of the ocean pH caused by the air-sea CO2 exchange with the globally well-mixed atmosphere [41]. We also found that pH reduction climate velocities are higher at high latitudes, which is consistent with [41] observations. Moreover, our results reveal a similar spatial distribution between the low climate velocities of pH reduction and those of oxygenation in the HCLME (Figures 2.4.1(e), (f), (h) and (i)). This result suggests a dynamic interplay between warming, deoxygenation, and pH changes in shaping oceanic conditions, highlighting the complexity of climate-induced changes in marine environments. In general, pH presents more climatic loss, followed by temperature and oxygen. Vertically (from 0 to 200m), temperature velocities decrease, and the highest speeds extend from the Equatorial Sector to the HCLME. On the other hand, climate velocities for pH maintain their magnitude range, but the velocities decrease near the coast. By contrast, the areas where the climate velocities for oxygen are slow at the subsurface are fast at the surface (Figure 2.4.1). In addition, the climate velocities for temperature show southward displacement, those for oxygen move northward, and those for pH do not show a uniform displacement pattern (Figure 2.4.2).

Regarding the focus zones, RN (SCCU) is the most (less) affected by deoxygenation; RN (SCCU), by pH reduction; and NCU (RN), by warming across all depths (Figure 2.4.3 and Table 2.4.1). In general, the island focal zones do not show a similar climate state. RN shows almost no climate conservation, high temperature and oxygen migration, and complete pH loss. By contrast, DA and JFA show conservation of subsurface oxygen but high overall climatic migration and pH loss. On the other hand, the upwelling zones show similar patterns, presenting oxygen conservation, pH migration, and temperature loss (Figure 2.4.3 and Table 2.9.4). SCCU presents

oxygen climate refugia across all depths. By contrast, NCU, DA and JFA present oxygen climate refugia, but only below the surface (100 and 200m), whereas RN shows oxygen climate refugia only at 100 m (Figures 2.4.3(d), (e) and (f)). Therefore, the least affected places are the upwelling areas off the continent's coast, followed by oceanic islands close to them (JFA and DA), and finally RN (the most affected zone, except for temperature). Hence, regions further out in the ocean could be more prone to CC. Based on the above, together with the fact that the HCLME is characterized by subsurface climate refugia for oxygen, and the slowest climate velocities for pH reduction, this region deserves priority for protection. Sections 2.7.2.1 and 2.7.2.2 describe in more detail the results of climate velocities and climatic state, respectively.

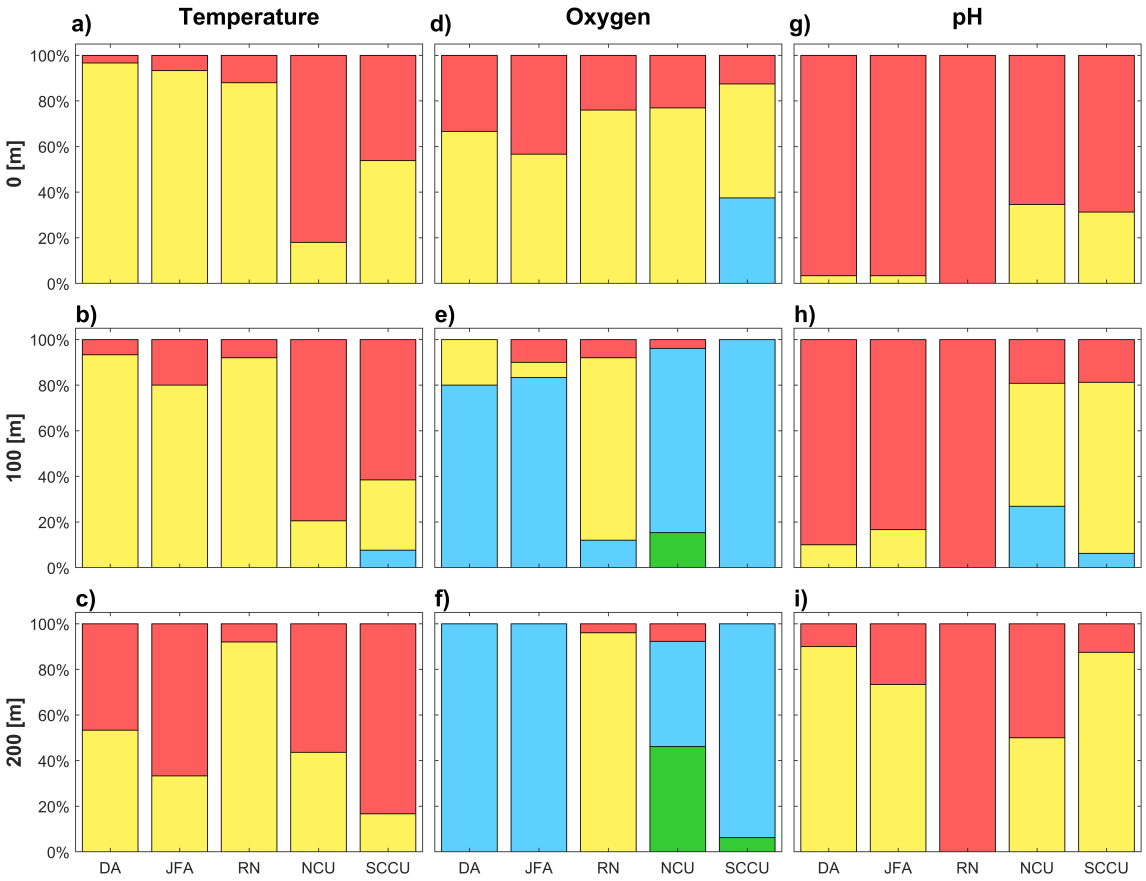

Figure 2.4.3: Stacked bar of climatic states percentages, for the "fossil-fueled" scenario (SSP5-8.5) at near future: 2015–2050, for the five focus zones (DA, JFA, RN, NCU, and SCCU) for temperature at (a) 0 m, (b) 100 m, (c) 200 m, oxygen at (d) 0 m, (e) 100 m, (f) 200 m, and pH at (g) 0 m, (h) 100 m, (i) 200 m. The colors represent climate conservation (cyan), climate migration (yellow), climate loss (dark orange), and climate oxygenation/cooling (green). The values are detailed in Table 2.9.4.

Table 2.4.1: Mean of climate velocities (with ± standard error from bootstrap resampling $n = 1000$) for the fossil-fueled scenario (SSP5-8.5) at near future: 2015–2050, across five zones (DA, JFA, RN, NCU, SCCU). * indicates values less than twice the standard error.

	Temperature			**Oxygen**			**pH**		
Depth (m)	0	100	200	0	100	200	0	100	200
DA	7.18 ± 0.25	4.71 ± 0.45	11.1 ± 0.89	-6.09 ± 0.58	-1.59 ± 0.97*	0.82 ± 2.03*	-31.88 ± 0.15	-27.76 ± 0.36	-6.98 ± 0.42
JFA	6 ± 0.33	5.37 ± 0.57	18.37 ± 0.9	-4.64 ± 0.67	-0.78 ± 1.25*	0.27 ± 1.89*	-29.07 ± 0.13	-15.26 ± 0.19	-4.82 ± 0.56
RN	7.07 ± 1.3	4.85 ± 0.58	3.66 ± 2.58*	-5.05 ± 2.52	-3.92 ± 0.92	-6.44 ± 2.07	-34.01 ± 0.41	-34.7 ± 4.23	-35.66 ± 4.18
NCU	6.9 ± 0.41	12.89 ± 0.7	6.47 ± 1.4	-20.59 ± 0.59	2.18 ± 0.65	3.32 ± 1.94*	-24.93 ± 0.27	-6.24 ± 0.28	-14.36 ± 0.52
SCCU	5.38 ± 0.48	8.74 ± 0.68	10.91 ± 1.55	-3.61 ± 0.64	0.02 ± 0.73*	1.45 ± 1.4*	-22.88 ± 0.23	-3.55 ± 0.26	-6.01 ± 0.58

2.4.2. Influence of climate scenarios on climate velocity

Climate velocity estimations highly depend on climate scenarios and periods. The "fossil-fueled" scenario presents higher climate velocities for warming and pH reduction than the "sustainability" scenario in the near future (2015–2050)—roughly twice as high at the surface (Figures 2.4.1 and 2.8.1)—and even higher at far future (2050–2100) (Figure 2.4.4). By contrast, the "sustainability" scenario presents higher climate velocities for deoxygenation than the "fossil-fueled" scenario in the near future, but lower in the far future (Figure 2.8.4). It is crucial to keep in mind that high climate velocities for deoxygenation indicate high displacement of oxygen climate with a tendency toward deoxygenation rather than high deoxygenation trends. Thus, the higher climate velocities of the "sustainability" scenario, compared to the "fossil-fueled" scenario, could be due to higher temporal trends or lower spatial gradients (Section 2.7.2.3 presents an analysis of the temporal trend and spatial gradient of oxygen, for both scenarios). The climate state analysis for the near future period illustrates how the "sustainability" scenario (Figure 2.8.2) results in greater conservation than the "fossil-fueled" scenario (Figure 2.4.2) for temperature and pH, but not for oxygen (Table 2.4.2, and Table 2.9.5). Both scenarios exhibit a similar spatial distribution of fastest velocities during the near future, but notable differences in the far future. The "sustainability" scenario reveals that FZs (except for temperature) almost disappear

in the far future but extend in the "fossil-fueled" scenario (Figure 2.4.4). Thus, while the "fossil-fueled" scenario shows more climatic changes over time, the "sustainability" scenario exhibits a contraction of FZs, presenting higher possibilities for preserving the climatic variables until the year 2100 [41] (see Section 2.7.2.4 for a more complete description).

Table 2.4.2: Percentages of climate conservation, migration, loss, and oxygenation/cooling presented in Figure 2.4.2.

	Temperature			**Oxygen**			**pH**		
Depth (m)	**0**	**100**	**200**	**0**	**100**	**200**	**0**	**100**	**200**
Conservation (%)	2.09	11.43	16.26	3.84	39.12	45.08	0	0.28	0
Migration (%)	62.66	59.25	50.06	62.69	49.34	40.29	4.24	13.96	18.91
Loss (%)	35.24	28.74	33.68	33.47	10.3	11.16	95.76	85.76	81.09
Oxygenation/cooling (%)	0	0.58	0	0	1.24	3.47	0	0	0

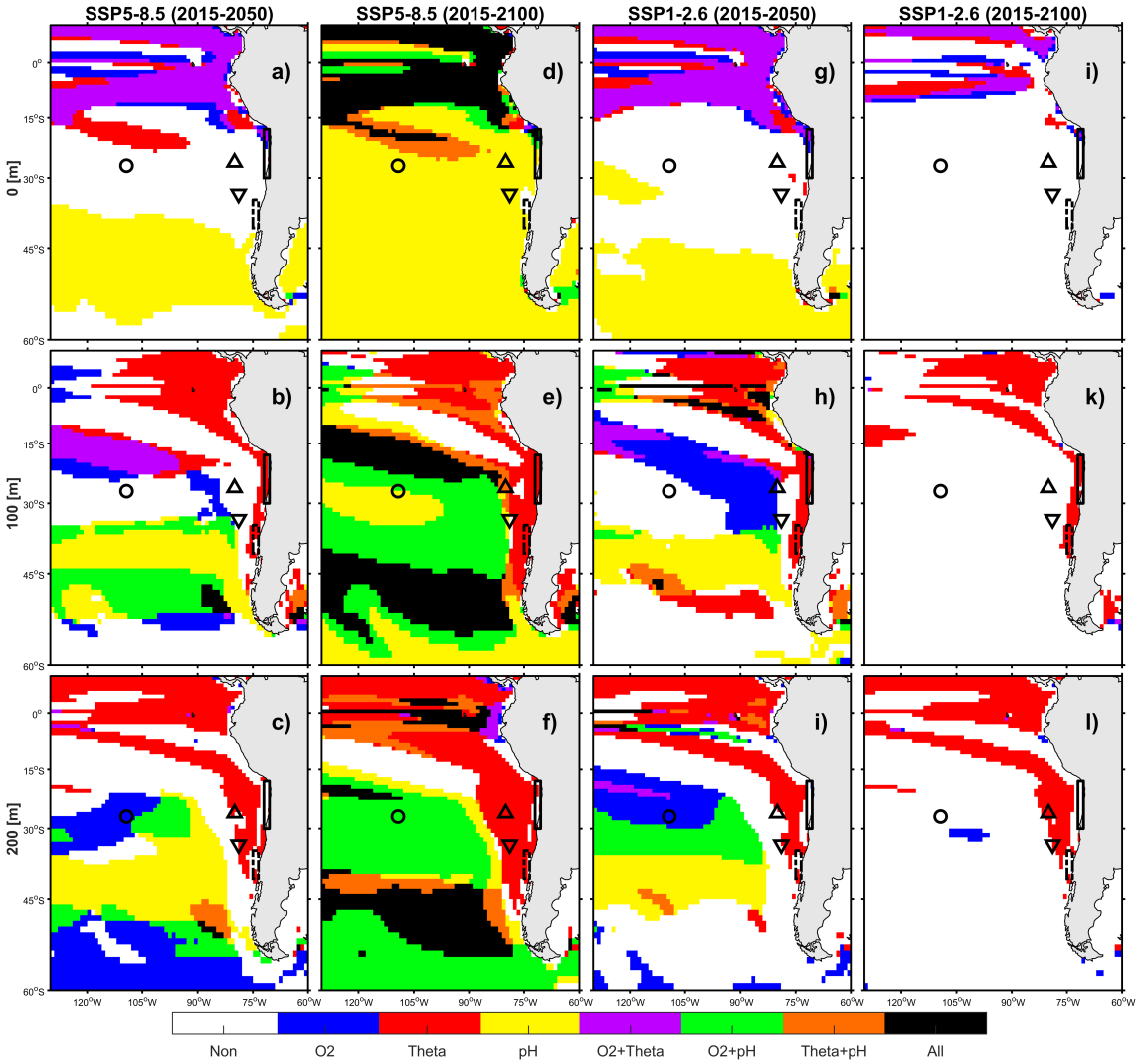

Figure 2.4.4: Fastest zones (FZ) for the "fossil-fueled" scenario (SSP5-8.5) for near future: 2015–2050 at (a) 0 m, (b) 100 m, (c) 200 m and for far future: 2015–2100 at (d) 0 m, (e) 100 m, (f) 200 m. FZ for the "sustainability" scenario (SSP1-2.6) for near future at (g) 0 m, (h) 100 m, and (i) 200 m, and for far future at (j) 0 m, (k) 100 m, and (l) 200 m. Colors represent areas where the climate velocities exceed the threshold of 25 % fastest velocities for near future (different for each scenario) defined in Table 2.3.1. Thus, color code classification follows as: oxygen (blue), temperature (red), pH (yellow), oxygen and temperature (purple), oxygen and pH (green), temperature and pH (orange), all of them (black), and none of them (white).

2.4.3. Limitations

According to [68], marine species follow the climate velocity displacement patterns with high accuracy. However, climate velocities illustrate a pattern of CC rather than directly indicating changes in species distribution, because they do not consider

any biological data, such as specific species' migration capacities. An advantage of climate velocity is the need for minimal information for its calculation. However, the sensitivity and tolerance of marine species should be incorporated into this framework for a quantitative estimate of the impact of CC on marine ecosystems. This limitation has been raised in previous CC studies based on climate velocities [5, 20, 42, 44, 46]. Physiological experiments should be conducted to assess key species' adaptation [69] and genetic plasticity across various life stages [70]. These experiments should focus on their responses to changes in temperature, pH, and oxygen concentration. By bridging the gap between climate models and biological responses, we can better anticipate and mitigate the impacts of CC on marine life [71, 72], by implementing ecosystem-protective fishing management techniques or establishing new MPAs.

Based on the coefficient of variation, climate velocities for temperature and pH show high homogeneity across models (Figures 2.8.5 and 2.8.7). However, the climate velocity for oxygen (Figure 2.8.6) below the surface (100 and 200 m) presents potential biases because of the high heterogeneity across models, which is consistent with previous studies [37, 43]. These uncertainties are higher under the "sustainability" scenario. This heterogeneity also affects the calculation of the oxygen FZ thresholds and mean climate velocities for the five focus zones (see the standard error in Table 2.3.1 and 2.4.1). ESM models are expected to show regional biases [73-76], which affect the mean gradients in water mass properties. Together with the low spatial resolution, and the smoothed ocean dynamics due to the averaging over time (and models), these limitations diminish the accuracy of the results. Nonetheless, ESM models are robust tools for simulating the current climate and are currently the best data source to study possible future CC repercussions, presenting more consistent results than biases.

2.4.4. Biological consequences

The climate velocities for warming, both at the surface over the continental shelf and in subsurface layers near ridges, could substantially impact marine fauna. Temperature is the primary environmental driver regulating metabolic rates, influencing survival, feeding, and growth [77]. Additionally, it affects gas solubility and the interaction of pH with species' physiology, potentially affecting population demography and community structure and increasing exposure to invasive species that are more tolerant to rising temperatures [77, 78]. The oxygen subsurface conditions appear

favorable for pelagic and benthic species residing in the OMZ because of climate conservation between 100 and 200 m. This could represent a climatic refuge for species tolerant to hypoxia. However, the synergistic effect of the "deadly trio" on fauna metabolism should be considered. The loss or migration of the climatic state of temperature and pH could reduce the environmental tolerance range to hypoxia, because the average oxygen demand of resident species would increase [72, 77, 79, 80]. In turn, this increase would lead to the migration of populations toward more favorable conditions, such as shifts to greater depths—a phenomenon that has been recorded during El Niño-Southern Oscillation (ENSO) events—ultimately resulting in changes in community structure within the OMZ [78, 81]. In the mesophotic communities of RN, the climate velocity results for oxygen and temperature are less concerning compared to those for pH. Habitat loss due to increased acidification represents a threat to mesophotic corals, potentially compromising the health of reef communities [82, 83]. Corals are habitat-forming species, providing refuge and food for diverse vertebrate and invertebrate taxa [84]. The degradation and mortality of mesophotic corals are already problems in RN, leading to the loss of biodiversity in these communities [85]. The subsurface oxygenation climate velocities in the OMZ (200 m) suggests a potential habitat expansion in the epipelagic zone (non-resident species) and the deepening of the OMZ, which could reduce the habitable space of epipelagic and benthic species within the OMZ ($<$200 m). On the continental shelf, demersal fish and crustacean fisheries are composed of species that inhabit the OMZ (cold, hypoxic, and low pH conditions), in whose core ($<$0.5 $\frac{ml}{L}$) these species' juveniles are recruited [81, 86-88]. Changes in oxygen, pH, and temperature conditions, such as the deepening of the oxycline during ENSO events, alter not only community composition but also recruitment patterns [81, 78]. A similar phenomenon could be expected in the Nazca and Juan Fernández ridges and the eastern portion of Salas y Gómez because those communities seem to be associated with subsurface hypoxic conditions [89]. Future studies should also consider the synergistic effect of the "deadly trio" on SEP habitability based on fauna metabolism.

2.5. Conclusions

Our study highlights the marked influence of climate change (CC) on marine ecosystem stressors in the southeastern Pacific (SEP) ocean, assessed through the unique lens of climate velocity [5, 42, 45, 46]. This tool allows us to identify regions

with rapid or slow climate changes, providing information about possible climatic loss and climatic refugia. The multi-stressor approach (i.e., the analysis of temperature, oxygen, and pH, three of the four major stressors suggested by [43]) and the multi-dimensional approach (different depths, periods, and climatic scenarios) enhance our understanding of the effects of CC. We identify areas resistant to CC and highlight their ecological importance. The coast of Peru-Chile (HCLME) at the subsurface presents oxygen climate refugia and the lowest pH reduction climate velocities, despite climatic loss of temperature. Temperature climatic refugia are present in southern Chile, and subsurface tropical ocean areas, notwithstanding the expected thermal expansion. Our analysis of the effects of CC on the focal zones suggests greater resistance to CC in regions near the coast. Thus, the region between the archipelagos and the upwelling systems may be a key zone for the conservation of marine life and deserves priority for protection. The comparative analysis of the two scenarios highlights that the "fossil-fueled" development pathway poses a great threat to marine environments, evidenced by the consistently higher climate velocities for warming and pH reduction. By contrast, this scenario exhibits greater oxygenation and lower deoxygenation climate velocities than the "sustainability" scenario, but only in the near future. However, the models show substantial variation, which diminishes the accuracy and dependability of the results for oxygen under the "sustainability" scenario. These findings emphasize the critical need for sustainable practices to mitigate adverse impacts. The chosen approach reveals potential future scenarios for habitat shifts and ecosystem changes and is a crucial resource for informing conservation strategies, sustainable fishing practices, and managing marine protected areas. By integrating these insights, we can better anticipate and prepare for the ecological consequences of CC, ultimately aiding in preserving and sustaining marine biodiversity in the SEP.

2.6. Acknowledgment

This research was funded by grant Fondecyt 1191606 and project R20F0008 Climate Action Planning (RL1 y RL 2) from the Centro de Estudios Avanzados en Zonas Áridas (CEAZA). In addition, we acknowledge the University of Concepción graduate grant in the framework of Geophysics master program, the support from Project Anillo BiodUCCT (ATE 220044), and the support from the Monitoring Program for Crustacean Fisheries of the Juan Fernández Archipelago (FIPA-2023-22).

2.7. Supplementary Text

2.7.1. Methods

This section illustrates important details about the methodology of the paper.

2.7.1.1. ScenariosMIP

1. The SSP1-2.6 scenario (Sustainability) assumes growth in sustainable and integrated development, respecting environmental limits. This scenario considers low challenges to mitigation and adaptation, and a 2.6 $\frac{W}{m^2}$ radiative forcing by the end of the century.

2. The SSP5-8.5 scenario (Fossil-fueled Development) assumes a competitive market future, aiming at rapid technological development for sustainability purposes, at the expense of exploiting fossil fuel resources due to lifestyles with high resource and energy consumption. This scenario implies a high challenge for mitigation but low adaptation, and an 8.5 $\frac{W}{m^2}$ radiative forcing by the end of the century [90-92].

2.7.1.2. Spatial gradient threshold selection

The average climate velocity for the focus zones was evaluated under different thresholds, and the results showed that there is no significant difference climate velocity for temperature between thresholds 0.0001 and 0.001, but that the values decline abruptly at thresholds 0.01 and 0.1. In the case of climate velocity for oxygen, there is no major difference between thresholds 0.0001, 0.001, and 0.01, but the values fall with threshold 0.1, while for climate velocity for pH the values fall to threshold 0.001 (Figure 2.8.3). Although there is no homogeneous behavior among different variables in the face of threshold changes; by having a sufficiently small threshold, the average values of the climate velocity stabilize (as is the case of oxygen between threshold 0.0001 and 0.01, or temperature between thresholds 0.0001 and 0.001). This is likely due to the threshold reaching (or near) a point that allows calculating the climate velocity by truncating the least amount of spatial gradient values, to obtain a relatively constant average climate velocity.

2.7.2. Results

This section provides a detailed description of the main results.

2.7.2.1. Climate Velocity in the SEP

For the "fossil-fueled" scenario (SSP5-8.5) in the near future (2015–2050), at the surface, the region between 10°N and 10°S (defined as the Equatorial Sector) shows the highest warming (positive) climate velocities (reaching values of up to 450 $\frac{km}{yr}$) (Figure 2.4.1(a)). At 100 m, the warming pattern is maintained in the equatorial sector (between 60 and 115°W), and another warming pattern emerges from the mainland coast to 80°W (HCLME). Low temperature climate velocities, and even cooling (negative) climate velocities are observed east of the Equatorial Sector (110 to 130°W; Figure 2.4.1(b)). At 200 m, a band of cooling climate velocities at 15°S (90 to 130°W) appears north of RN. Warming is observed in the Equatorial Sector (along with the entire longitudinal band) and the HCLME, covering DA, JFA, NCU, and SCCU (Figure 2.4.1(c)). On the surface, the climate velocity for oxygen behaves very similarly to the climate velocity for temperature. The highest climate velocity for deoxygenation (negative) are found in the Equatorial Sector, with maximum values above -700 $\frac{km}{yr}$ (Figure 2.4.1(d)). At 100 m, the zones with the highest deoxygenation velocities are found west of the equatorial sector (120 to 130°W) and north of RN. The HCLME shows low oxygenation (positive) climatic velocities (Figure 2.4.1(e)). At 200 m the areas with the highest deoxygenation climate velocities are located mainly to the west of RN (between 120 and 130°W), and between 55 and 60°S. The HCLME shows oxygenation climate velocities and the lowest deoxygenation climate velocities, like 100 m, but with more extension to the west (Figure 2.4.1(f)). The climate ranges for pH are notably narrower, and always negative. . At the surface, the highest velocities are found around 30°S to 60°S. There are two low climate velocity cores associated to the north of the SCCU and northwest of NCU (Figure 2.4.1(g)). At 100 m, the low climate velocity zone located in NCU and SCCU extends along the HCLME, reaching JFA, and almost reaching DA (Figure 2.4.1(h)). At 200 m, the low climate velocity zone in the HCLME disappears from NCU, and extends westward, covering the islands (JFA and DA, Figure 2.4.1(i)). By comparing the spatial distribution of climate velocities of the "sustainability" scenario (Figure 2.8.1) with the "fossil-fueled" scenario at the near future (figure 2), we found that they are very similar for every case, but the magnitude differs. The highest warming

climate velocities (positive) are 256, 56, and 34 $\frac{km}{yr}$ slower (for 0, 100 and 200 m, Figures 2.8.1(a), (b), and (c)) than the "fossil-fueled" scenario, and it doesn´t present negative values (cooling climate velocities), except in a few cells at 200 m (Figure 2.8.1(c)). The highest deoxygenation climate velocities (negative) are 90, 40, and 10 $\frac{km}{yr}$ faster (for 0, 100 and 200 m, Figures 2.8.1(d), (e), and (f)) than the "fossil-fueled" scenario. The range of the pH climate velocities at the "sustainability" scenario is narrower. The highest pH reduction climate velocities (negative) are 19, 18, and 14 $\frac{km}{yr}$ slower (for 0, 100 and 200 m, Figures 2.8.1(g), (h), and (i), and at the surface the lowest climate velocity for pH reduction is 7 $\frac{km}{yr}$ slower (Figure 2.8.1(g)) than the "fossil-fueled" scenario.

2.7.2.2. Climate state for the SEP and focus zones

For the "fossil-fueled" scenario in the near future, surface temperature presents climatic loss (35.24 %) in most Equatorial Sector, and toward the DA and JFA islands, but not reaching them, and the HCLME. However, the southern sector of the mainland shows climatic conservation (2.09 %), while everything else is climatic migration (62.66 %). The direction of displacement is generally southward, with a slight inclination toward DA and JFA, from the Equatorial sector (Figure 2.4.2(a)). At 100 m, the main trends remain the same (59.25 % migration, 28.74 % loss), except for a climatic conservation (11.43 %) and cooling (0.58 %) sector to the west of the Equatorial sector, which expands from the west to the southeast, in the direction of the NCU. The direction of displacement is maintained, except for the sectors close to the conservation zone, which move towards it (Figure 2.4.2(b)). At 200 m the climatic conservation sector (16.26 %) to the west disappears, but others appear at 10°S, from 130°W to the east of RN, and the south of Chile. On the other hand, the climatic loss pattern (33.68 %, 50.06 % climatic migration) of the HCLME expands westward (Figure 2.4.2(c)). Oxygen at the surface is like temperature (62.69 % migration, 33.47 % loss), but with more conservation zones (at 55°S and SCCU, 3.8 %). The climatic displacement direction is the same as in the case of surface temperature, but between 12 and 60°S, the direction is the opposite (Figure 2.4.2(d)). On the other hand, at 100 m, the classifications are almost opposite to the temperature case. There is a high presence of climatic conservation areas (39.12 %) and small climatic oxygenation zones (1.24 %) in the Equatorial Sector and the HCLME, covering DA, JFA, NCU, and SCCU. The rest of the map mostly shows climatic migration (49.34 %, 10.3 % loss). The trend of the direction of displacement is northward and towards

the climatic conservation zone (Figure 2.4.2(e)). At 200 m the climatic conservation zone (45.1 %) expands westward, decreasing the climatic migration zones (41.9 %), but disappears from 55°S, being replaced by a climatic loss zone (12 %). The climatic oxygenation zones almost tripled in size. The direction of displacement is maintained (Figure 2.4.2(f)). The pH shows almost complete climatic loss at the surface (95.76 %, 4.24 % climatic migration) and no general directional trend of displacement (Figure 2.4.2(g)). At 100 m, a small zone of climatic conservation (0.28 %) appears in NCU and SCCU. In addition, a zone of climatic migration (13.96 %, 85.76 % climatic loss) appears at 5°N and between NCU and SCCU, which expands northwesterly to 2°S. At this depth, there is a more pronounced trend in displacement toward the coastal and equatorial sectors (Figure 2.4.2(h)). At 200 m, climatic conservation zones disappear, and climatic migration zones expand slightly (18.91 %, 81.09 % climatic loss). The direction of displacement shows a greater tendency toward the HCLME (Figure 2.4.2(i)). See the percentages detailed in Table 2.4.2.

DA only shows climate conservation for oxygen at 100 (80 %, Figure 2.4.3(e)) and 200 m (100 %, Figure 2.4.3(f)). Climate migration is higher on temperature at all depths (96.67 %, 93.33 % and 53.33 % at 0, 100, and 200 m; Figures 2.4.3(a), (b), and (c)), on pH at 200 m (90 %, Figure 2.4.3(j)), and oxygen at 0 m (66,67 %, Figure 2.4.3(d)). Climate loss is higher on pH at 0 (96.67 %, Figure 2.4.3(g)) and 100 m (90 %, Figure 2.4.3(h)), and temperature at 200 m (46.67 %, Figure 2.4.3(c)). JFA is like DA in most cases, but has slight differences, such as lower climate migration, and higher climate loss. RN on the other hand, presents just 12 % of climate conservation, just for oxygen at 100 m (Figure 2.4.3(e)), high (low) climatic migration (loss) in all cases, except for pH at all depths (100 % climatic loss; Figures 2.4.3(g), (h), and (j)). NCU presents high climatic oxygenation at 200 m (46.15 %) and in lower percentage at 100 m (15.38 %), climatic conservation in oxygen at 100 (80.77 %, Figure 2.4.3(e)) and 200 m (46.15 %, Figure 2.4.3(f)), and in pH at 100 m (26.92 %, Figure 2.4.3(h)), climate migration almost all cases, and is higher in oxygen (76.92 %, Figure 2.4.3(d)) at 0 m, pH at 100 m (53.85 %, Figure 2.4.3(h)), and temperature at 100 m (43.59 %, Figure 2.4.3(b)). NCU climatic loss is present in all cases, but higher in temperature at all depths (82.05 %, 79.40 %, and 56.41 % at 0, 100 and 200 m; Figures 2.4.3(a), (b) and (c)), and pH at surface (65.38 %, Figure 2.4.3(g)). SCCU is the zone that presents most climatic conservation, with higher levels in oxygen (37.5 %, 100 %, and 93.75 % at 0, 100 and 200 m; Figures 2.4.3(d), (e) and (f)), but lower in temperature (7.69 %,

Figure 2.4.3(b)) and pH at 100 m (6.25 %, Figure 2.4.3(h)). This zone also presents climatic oxygenation, but less than NCU (6.25 % at 200 m). Climate migration values are higher in pH at 100 (75 %, Figure 2.4.3(h)) and 200 m (87.5 %, Figure 2.4.3(i)), and temperature (53.85 %, Figure 2.4.3(a)) and oxygen (50 %, Figure 2.4.3(d)) at surface. Climate loss is higher in temperature (46.15 %, 61.54 %, and 83.33 % at 0, 100 and 200 m; Figures 2.4.3(a), (b) and (c)) and in pH at 0 m (68.75 %, Figure 2.4.3(g)). See the percentages detailed in Table 2.9.4.

The Climate state for the "sustainability" Scenario, at the near future (Figure 2.8.2), is considerably different from the "fossil-fueled" scenario. For temperature, two conservation zones remain across all depths, covering from 50 to 60°S, and around RN, from 80 to 130°W (Figures 2.8.2(a), (b), and (c)). The equatorial sector also presents a conservation zone, but just at 100 m (Figure 2.8.2(b)). The temperature in this scenario presents 36.2 %, 28.65 % and 19.47 % (0, 100 and 200 m respectively) more conservation than the "fossil-fueled" scenario (Tables 2.4.2 and 2.9.5). The oxygen presents almost the same conservation zones that temperature at the surface (Figure 2.8.2(d)), but at 100 m almost vanishes (Figure 2.8.2(e)), with 24.2 % less than the oxygen at 100 m in the "fossil-fueled" scenario (Tables 2.4.2 and 2.9.5). At 200 m (Figure 2.8.2(f)) the conservation zone is also narrower compared to the "fossil-fueled" scenario (by 21.71 %, Tables 2.4.2 and 2.9.5). The pH is similar in both scenarios but presents a larger conservation zone in the HCLME by 2.27 and 0.74 % (Tables 2.4.2 and 2.9.5) at 100 and 200 m (Figures 2.8.2(h) and (i)).

2.7.2.3. Why are there higher deoxygenation climate velocities in the "sustainability" scenario?

While the rates of warming and pH reduction are higher in the Fossil-fuel scenario than the "sustainability" scenario for all cases, the rate of deoxygenation climate velocities in the "sustainability" scenario at the near future exceeds the Fossil-fuel scenario by about 100 (0 m), 40 (100 m) and 10 $\frac{km}{yr}$ (200 m, figure 2). We should remember that these values do not necessarily mean that there will be greater deoxygenation in the "sustainability" scenario, but that its climatic displacement will be greater. The climate velocity corresponds to a ratio between the temporal trend and the spatial gradient, thus high values may be due to either a high temporal trend or a low spatial gradient. We compare both the oxygen temporal trend and the spatial gradient for both scenarios in two cases: 1) when the climate velocity

for deoxygenation is higher in the "sustainability" scenario than in the "fossil-fueled" scenario (Figure 2.8.8), and 2) when it is lower (Figure 2.8.9). In the first case (higher climate velocity for deoxygenation in the "sustainability" scenario), on the surface, the deoxygenation temporal trend (negative temporal trend) is higher (more negative) in the Fossil-fuel scenario, but the spatial gradient is smaller for the "sustainability" scenario. In other words, even while the Fossil-fuel scenario exhibits a larger deoxygenation temporal trend, the "sustainability" scenario's spatial gradient is sufficiently low to leads to a higher climate velocity for the "sustainability" scenario (Figures 2.8.8(a) and (d)). In the case of 100 and 200 m, the spatial gradient is similar in both scenarios (Figures 2.8.8(e) and (f)), but the deoxygenation temporal trend is approximately double in the "sustainability" scenario (Figures 2.8.8(b) and (c)), i.e., there is a greater temporal trend of deoxygenation in the "sustainability" scenario at these depths. For the second case (higher climate velocity for deoxygenation in the "fossil-fueled" scenario), the spatial gradient is similar between scenarios, at all depths, but the temporal trend of deoxygenation is always greater (more negative) for the "fossil-fueled" scenario (Figure 2.8.9).

2.7.2.4. Fastest zones in the SEP

For the "fossil-fueled" scenario in the near future, at the surface, the Equatorial Sector hosts the deoxygenation fastest zones (DFZ) and warming fastest zones (WFZ), reaching a part of the NCU, while the pH fastest zones (PFZ) is between 37 to 55°S (Figure 2.4.4(a)). At 100 m, the WFZ is bounded to the east, extending along the HCLME, covering the NCU and SCCU, and non-continuously to the north of RN, overlapping with a DFZ, which also extends from 36 to 53°S with the PFZ (Figure 2.4.4(b)). At 200 m, the WFZ extends over the entire Equatorial Sector, and across the HCLME to 45°S, covering JFA and DA. The PFZ slightly approaches near RN. The DFZ splits, covering RN and extending from 46 to 60°S (Figure 2.4.4(c)). Compared to the far future (2015–2100) at the surface, the DFZ keeps its spatial distribution, the WFZ slightly expands, and the PFZ extends over the entire domain (Figure 2.4.4(d)). At 100 m, the WFZ expands from the coast to 130°W (around the 15°S and 45°S), the DFZ expands to the center of the map, reaching RN, and the PFZ expands from 15 to 60°S, outside the HCLME and the Equatorial Sector (Figure 2.4.4(e)). Compared to the 200 m, the PFZ remains almost equal, but disappears from the Equatorial Sector, the DFZ slightly moves southward, and the WFZ expands over the entire Equatorial Sector and nearly vanishes at 15°S (Figure 2.4.4(f)). The

"sustainability" scenario in the near future presents spatial FZ patterns that closely resemble those of "fossil-fueled" scenario, albeit with some minor deviations. However, when we shift our focus to the far future, we observe a significant reduction in all FZ's, with some experiencing more drastic changes than others. The PFZ completely disappears at all depths, while the DFZ only makes a faint appearance at the surface in the northern sector. At 100 and 200 m, only small traces of the DFZ remain. In contrast, the WFZ stands out as the only one that remains prevalent.

When we compare the percentile value that determines the WFZ, in the "fossil-fueled" scenario is 173 % (0 m), 71 % (100 m), and 37 % (200 m) higher than in the "sustainability" scenario. In the case of DFZ, the threshold of the "fossil-fueled" scenario is higher than the "sustainability" scenario only at the surface (53.5 %). While with increasing depth, the threshold is higher for the "sustainability" scenario with 35 % and 40 % for 100 and 200 m respectively, a significant contrast between the two scenarios. For PFZs, in the "fossil-fueled" scenario, the percentile values are 102 %, 95 %, and 75 % higher than the "sustainability" scenario, for 0, 100, and 200 m, respectively (Table 2.3.1).

2.8. Supplementary Figures

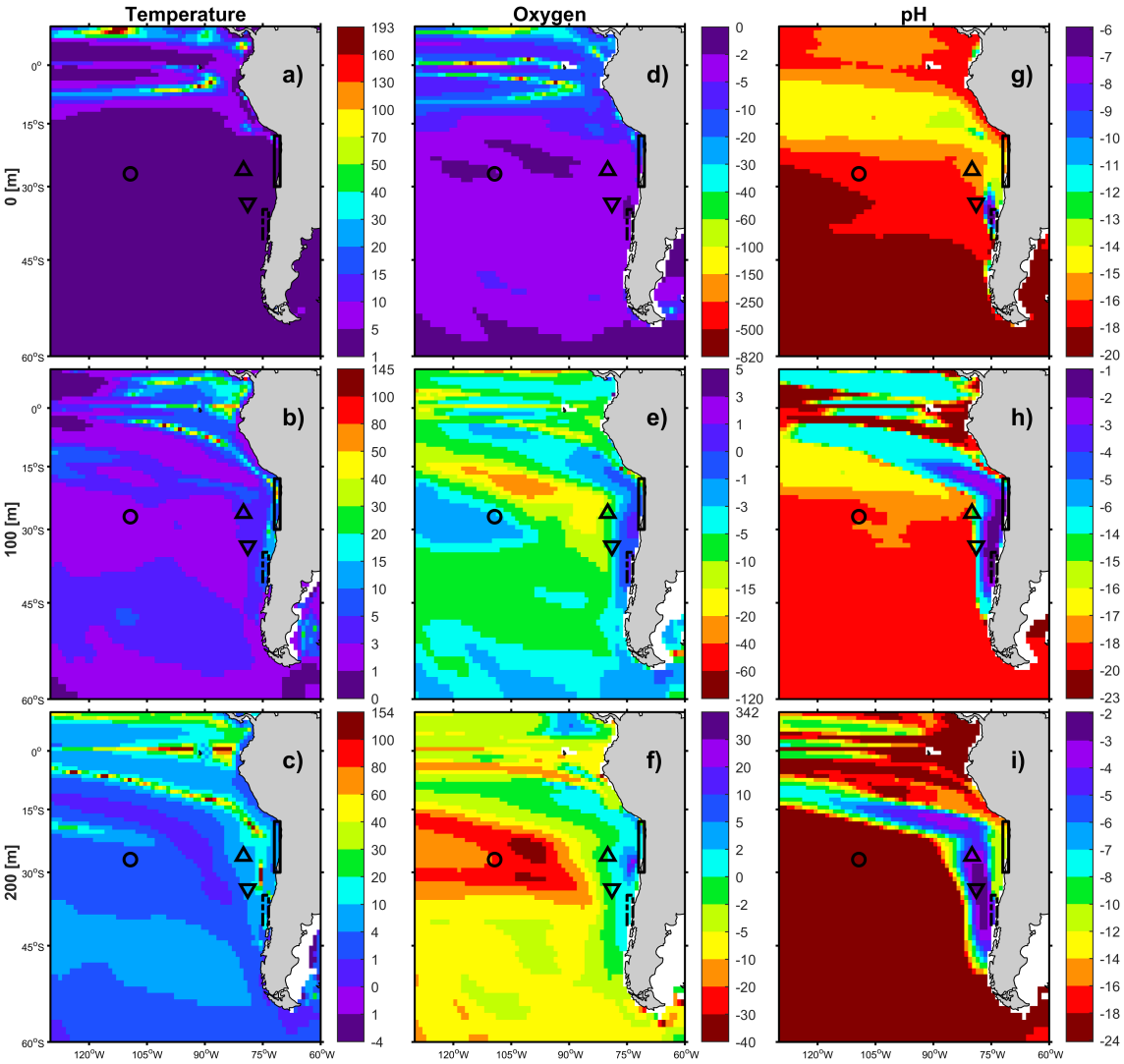

Figure 2.8.1: Climate velocities ($\frac{km}{yr}$) for the "sustainability" scenario (SSP1-2.6) at near future: 2015–2050, for temperature at (a) 0 m, (b) 100 m, (c) 200 m depth, oxygen at (d) 0 m, (e) 100 m, (f) 200 m depth, and pH at (g) 0 m, (h) 100 m, (i) 200 m.

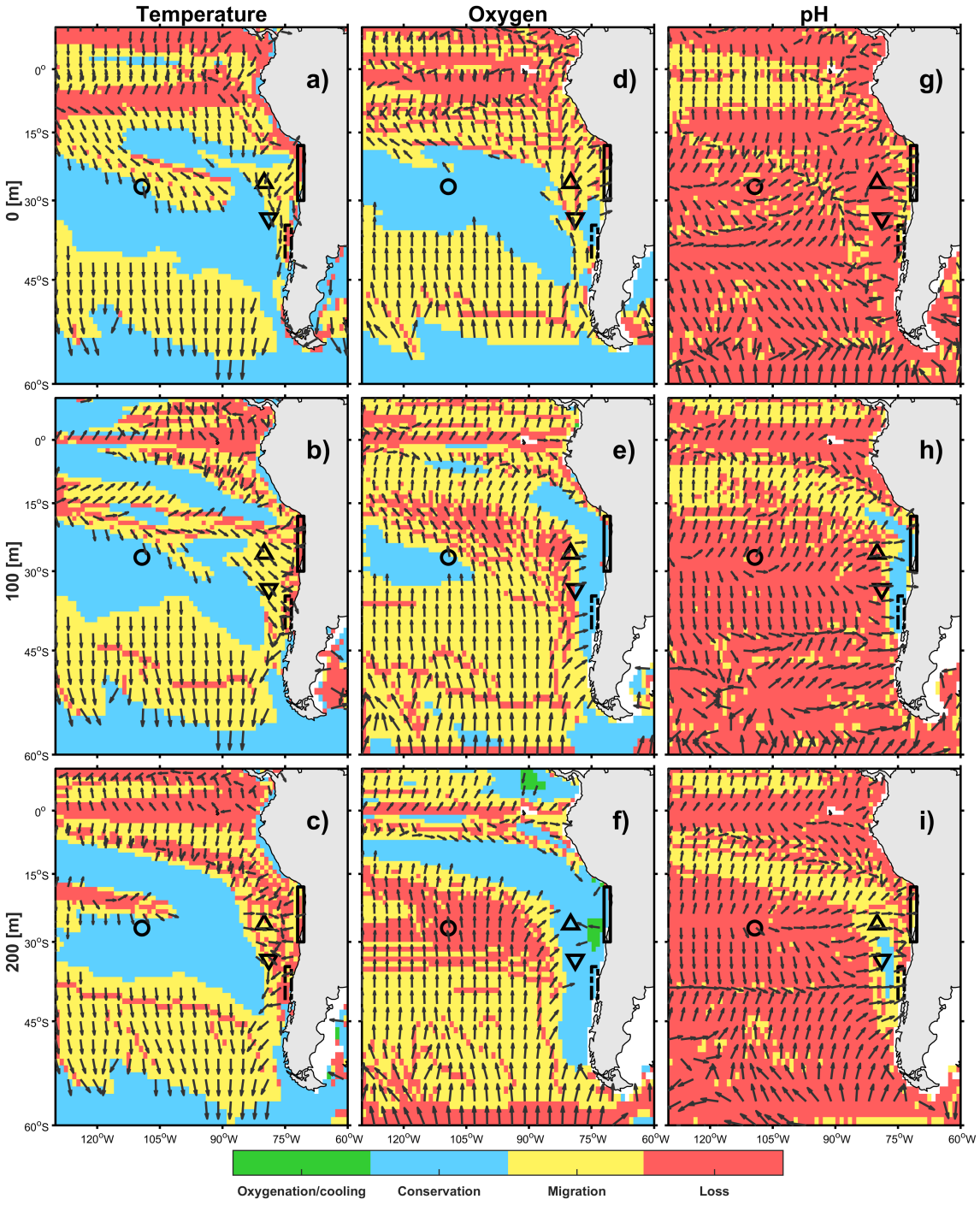

Figure 2.8.2: Climate state for the "sustainability" scenario (SSP1-2.6) at near future: 2015–2050, for temperature at (a) 0 m, (b) 100 m, (c) 200 m, oxygen at (d) 0 m, (e) 100 m, (f) 200 m, and pH at (g) 0 m, (h) 100 m, (i) 200 m. The colors represent climate conservation (cyan), climate migration (yellow), and climate loss (dark orange).

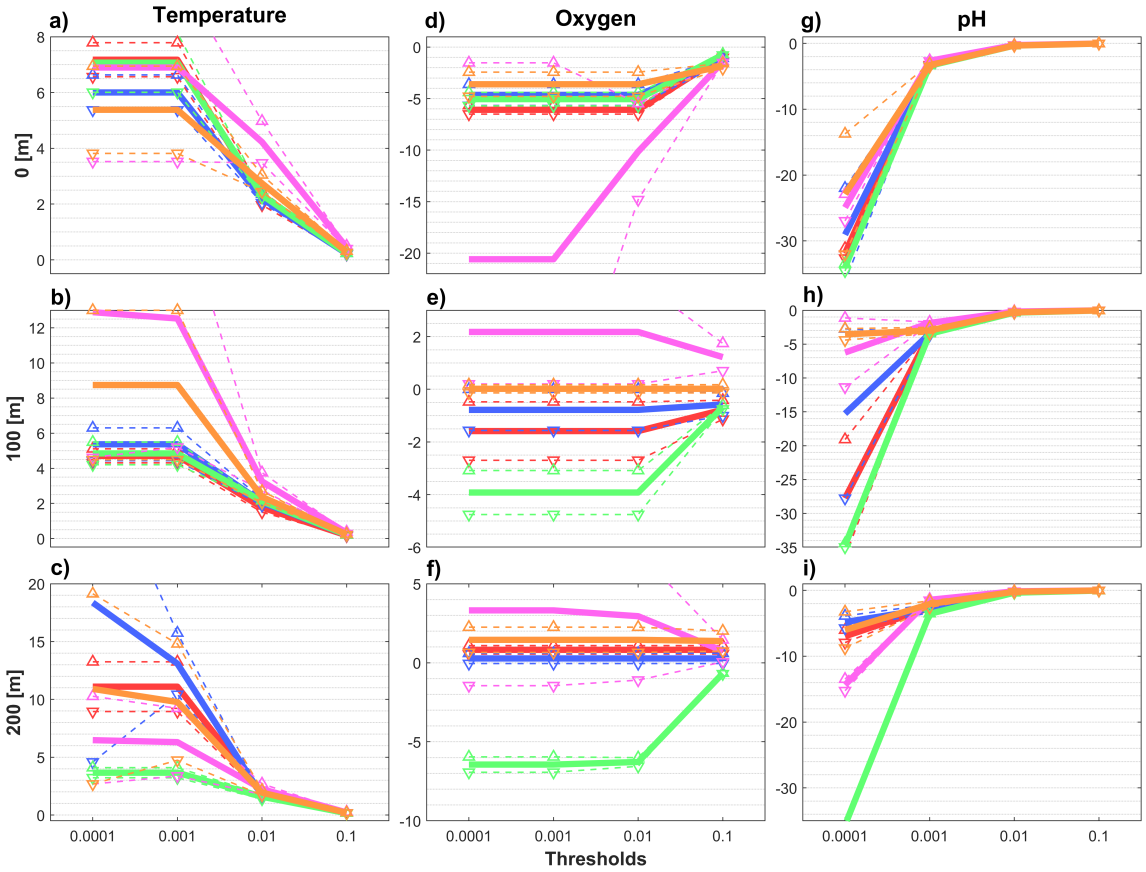

Figure 2.8.3: Mean climate velocities of the five focal zones under four spatial gradient thresholds, for the "fossil-fueled" scenario (SSP5-8.5) at near future: 2015–2050, for temperature at (a) 0 m, (b) 100 m, (c) 200 m depth, oxygen at (d) 0 m, (e) 100 m, (f) 200 m depth, and pH at (g) 0 m, (h) 100 m, (i) 200 m depth. Dashed lines represent the standard deviation above (upward triangle) and below (downward triangle) the mean values. Colors represent the five focal zones, DA (red), JFA (blue), RN (green), NCU (pink), SCCU (orange).

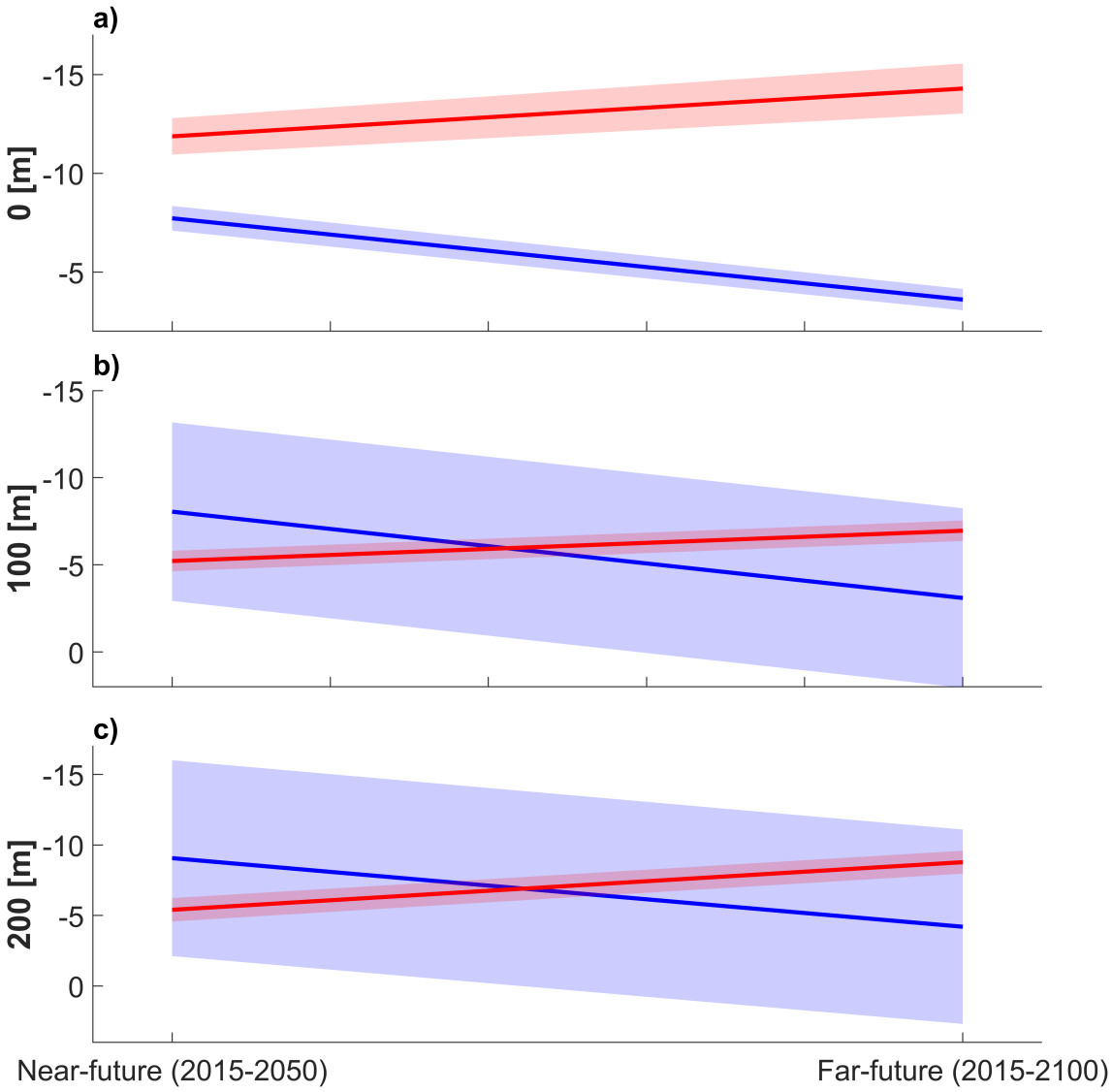

Figure 2.8.4: Percentile 25th (with ± associated standard error estimate by bootstrap resampling n=1000) of oxygen climate velocities at (a) 0 m, (b) 100 m and (c) 200 m, for the "fossil-fueled" scenario (SSP5-8.5; red) and the "sustainability" scenario (SSP1-2.6; blue), at near future: 2015–2050, and far future: 2015–2100. This percentile defines the fastest 25 % oxygen climate velocities.

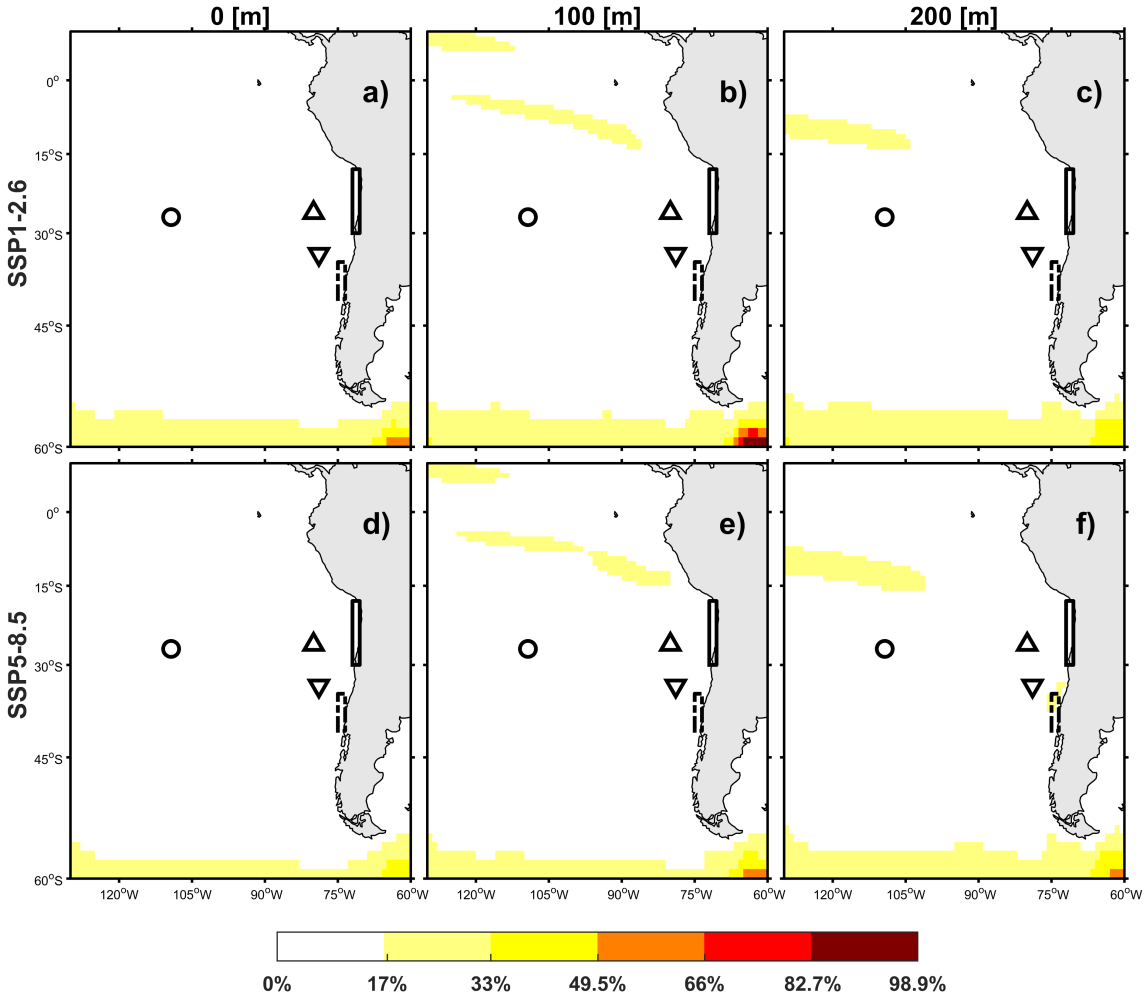

Figure 2.8.5: Coefficient of variation (percentage) of temperature, for the "sustainability" scenario at (a) 0 m, (b) 100 m and (c) 200 m, and for the "fossil-fueled" scenario at (d) 0 m, (e) 100 m and (f) 200 m. This shows the homogeneity (0 %) or heterogeneity across model outputs.

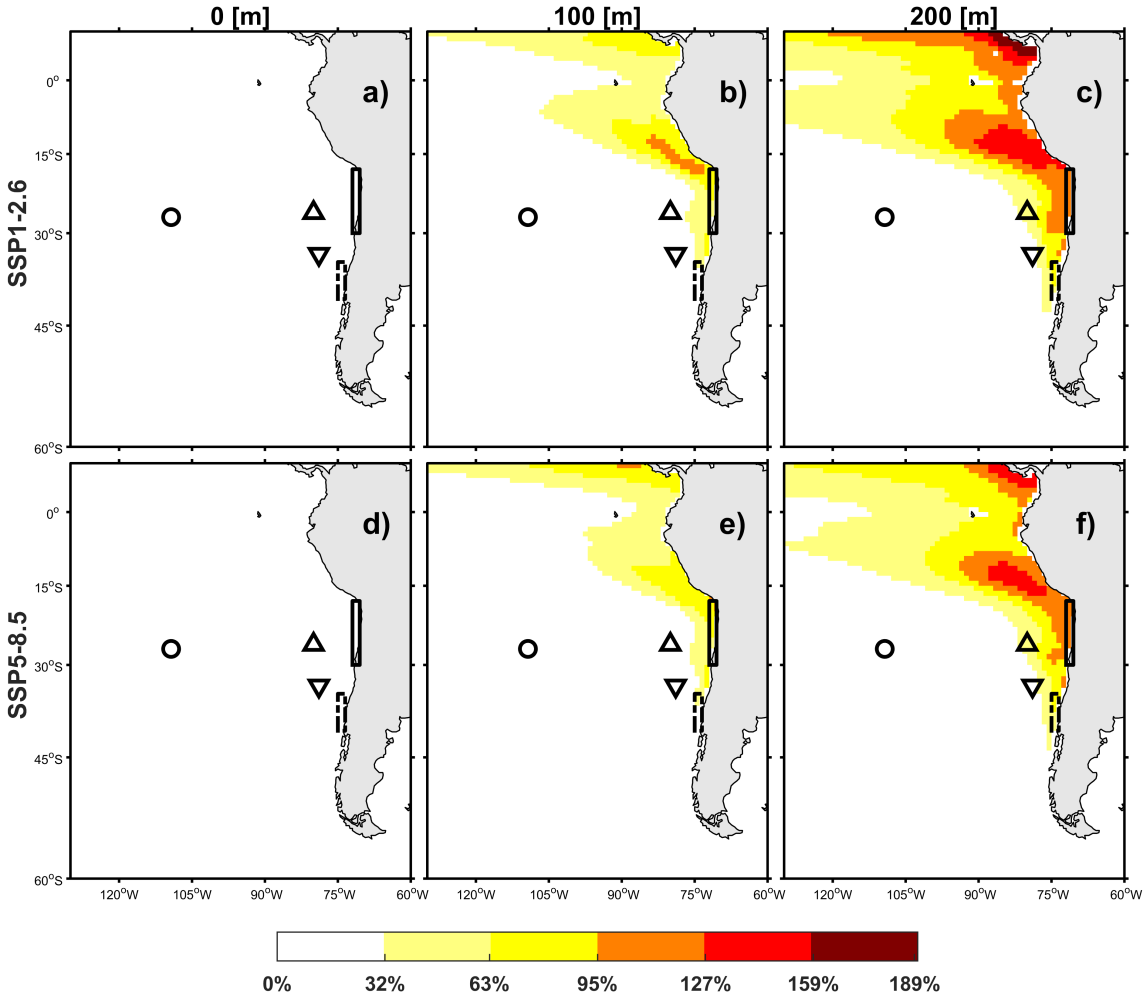

Figure 2.8.6: Coefficient of variation (percentage) of oxygen, for the "sustainability" scenario at (a) 0 m, (b) 100 m and (c) 200 m, and for the "fossil-fueled" at (d) 0 m, (e) 100 m and (f) 200 m. This shows the homogeneity (0 %) or heterogeneity across model outputs.

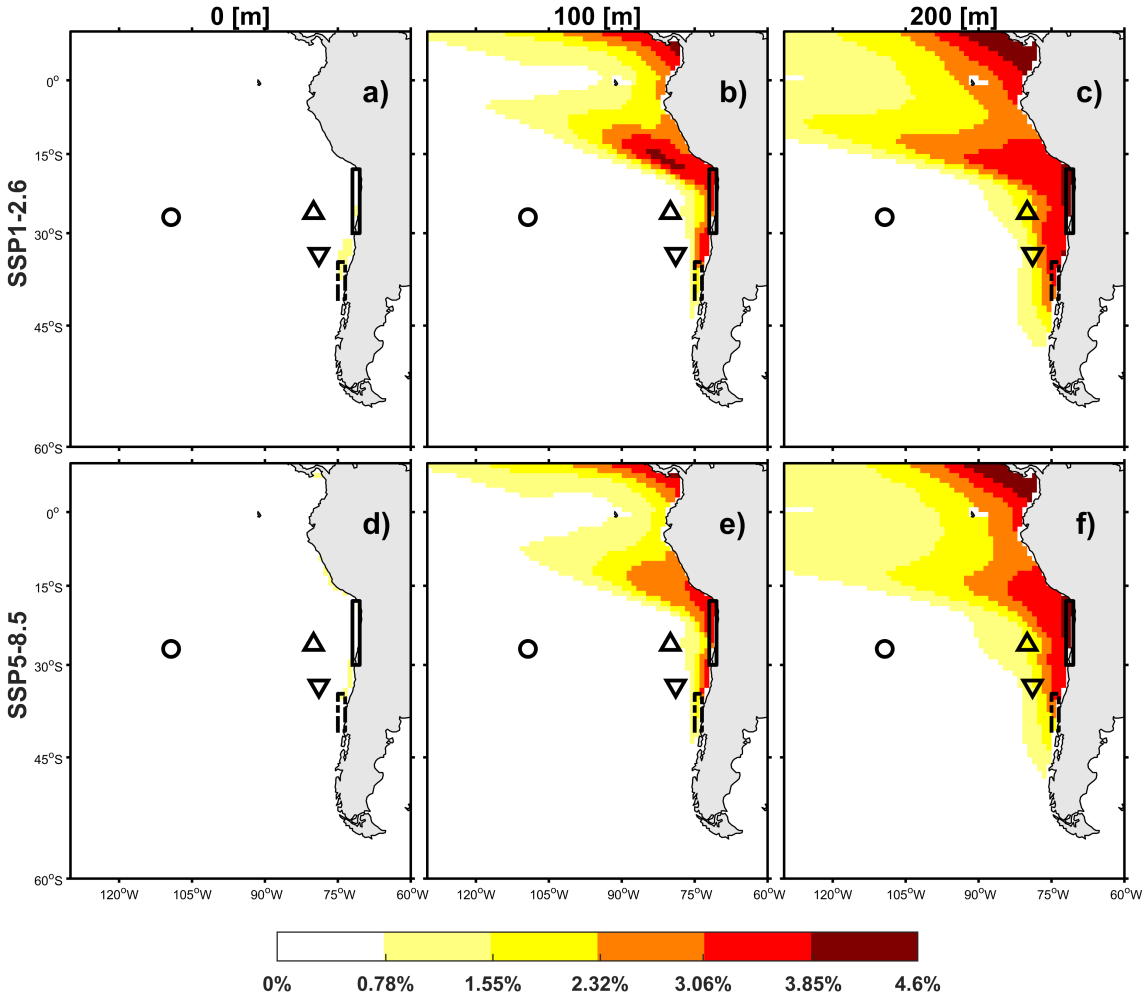

Figure 2.8.7: Coefficient of variation (percentage) of pH, for the "sustainability" scenario at (a) 0 m, (b) 100 m and (c) 200 m, and for the "fossil-fueled" at (d) 0 m, (e) 100 m and (f) 200 m. This shows the homogeneity (0 %) or heterogeneity across model outputs.

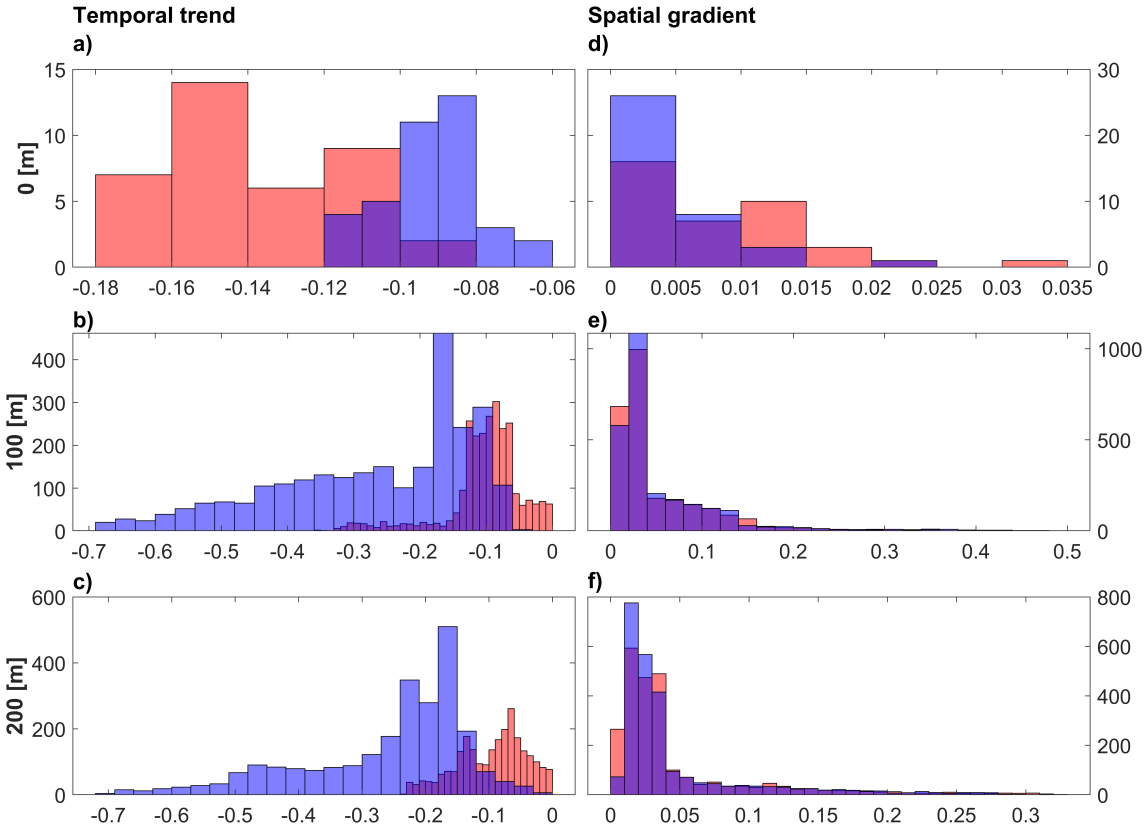

Figure 2.8.8: Distribution of the oxygen temporal trend (mmol m^{-3} yr^{-1}) at (a) 0 m, (b) 100 m and (c) 200 m, and spatial gradient (mmol m^{-3} km^{-1}) at (d) 0 m, (e) 100 m and (f) 200 m, for the cells where the climate velocity for deoxygenation is higher on the "sustainability" scenario than the "fossil-fueled" scenario, at the near future. The blue bars represent the "sustainability" scenario, and the red bars represent the "fossil-fueled" scenario. There are 38 values for 0 m, 2590 for 100 m and 2469 for 200 m.

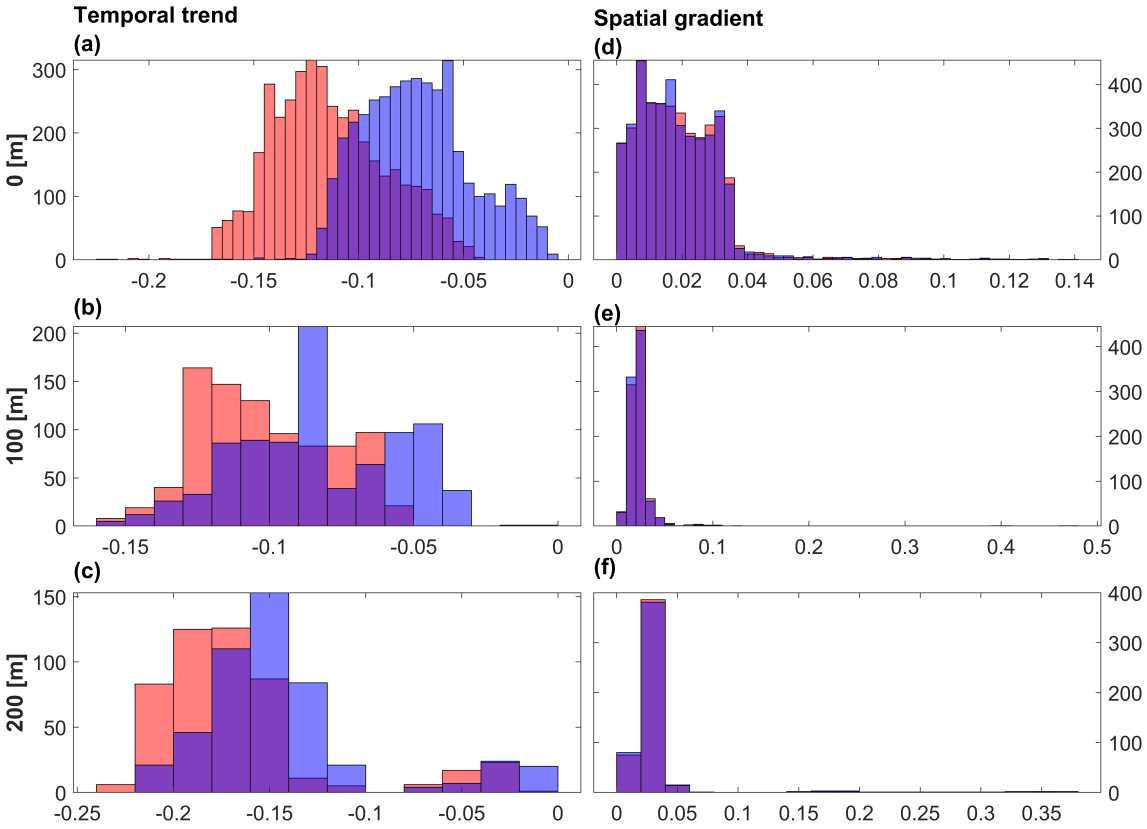

Figure 2.8.9: Distribution of the oxygen temporal trend (mmol m^{-3} yr^{-1}) at (a) 0 m, (b) 100 m and (c) 200 m, and spatial gradient (mmol m^{-3} km^{-1}) at (d) 0 m, (e) 100 m and (f) 200 m, for the cells where the climate velocity for deoxygenation is lower on the "sustainability" scenario than the "fossil-fueled" scenario, at the near future. The blue bars represent the "sustainability" scenario, and the red bars represent the "fossil-fueled" scenario. There are 3972 values for 0 m, 889 for 100 m and 490 for 200 m.

2.9. Supplementary Tables

Table 2.9.1: Model outputs for the "fossil-fueled" scenario (SSP5-8.5).

Variable	Model	Variant label	DOI
Thetao	BCC BCC-CSM2 MR	r1i1p1f1	http://doi.org/10.22033/ESGF/CMIP6.3050
Thetao	CAMS CAMS-CSM1.0	r1i1p1f1	http://doi.org/10.22033/ESGF/CMIP6.11052

Variable	Model	Variant label	DOI
Thetao	CCCma CanESM5	r8i1p2f1	http://doi.org/10.22033/ESGF/CMIP6.3696
Thetao	CCCma CanESM5-CanOE	r1i1p2f1	http://doi.org/10.22033/ESGF/CMIP6.10276
Thetao	CMCC CMCC-ESM2	r1i1p1f1	http://doi.org/10.22033/ESGF/CMIP6.13259
Thetao	CNRM-CERFACS CNRM-CM6-1	r1i1p1f2	http://doi.org/10.22033/ESGF/CMIP6.4224
Thetao	CNRM-CERFACS CNRM-ESM2-1	r5i1p1f2	http://doi.org/10.22033/ESGF/CMIP6.4226
Thetao	E3SM-Project E3SM-1.0	r3i1p1f1	http://doi.org/10.22033/ESGF/CMIP6.15178
Thetao	INM INM-CM4-8	r1i1p1f1	http://doi.org/10.22033/ESGF/CMIP6.12337
Thetao	INM INM-CM5-0	r1i1p1f1	http://doi.org/10.22033/ESGF/CMIP6.12338
Thetao	IPSL IPSL-CM6A-LR	r14i1p1f1	http://doi.org/10.22033/ESGF/CMIP6.5271
Thetao	MIROC MIROC-ES2L	r1i1p1f2	http://doi.org/10.22033/ESGF/CMIP6.5770
Thetao	MIROC MIROC6	r12i1p1f1	http://doi.org/10.22033/ESGF/CMIP6.5771
Thetao	MOHC HadGEM3-GC31-LL	r2i1p1f3	http://doi.org/10.22033/ESGF/CMIP6.10901
Thetao	MOHC UKESM1.0-LL	r1i1p1f2	http://doi.org/10.22033/ESGF/CMIP6.6405

Variable	Model	Variant label	DOI
Thetao	MRI MRI-ESM2.0	r1i1p1f1	http://doi.org/10.22033/ESGF/CMIP6.6929
Thetao	NCAR CESM2	r11i1p1f1	http://doi.org/10.22033/ESGF/CMIP6.7768
O2	CCCma CanESM5	r8i1p2f1	http://doi.org/10.22033/ESGF/CMIP6.3696
O2	CCCma CanESM5-CanOE	r3i1p2f1	http://doi.org/10.22033/ESGF/CMIP6.10276
O2	CMCC CMCC-ESM2	r1i1p1f1	http://doi.org/10.22033/ESGF/CMIP6.13259
O2	CNRM-CERFACS CNRM-ESM2-1	r2i1p1f2	http://doi.org/10.22033/ESGF/CMIP6.4226
O2	IPSL IPSL-CM6A-LR	r2i1p1f1	http://doi.org/10.22033/ESGF/CMIP6.5271
O2	MIROC MIROC-ES2L	r1i1p1f2	http://doi.org/10.22033/ESGF/CMIP6.5770
O2	MOHC UKESM1.0-LL	r1i1p1f2	http://doi.org/10.22033/ESGF/CMIP6.6405
O2	MRI MRI-ESM2.0	r1i2p1f1	http://doi.org/10.22033/ESGF/CMIP6.6929
O2	NCAR CESM2	r11i1p1f1	http://doi.org/10.22033/ESGF/CMIP6.7768
O2	NCC NorESM2-LM	r1i1p1f1	http://doi.org/10.22033/ESGF/CMIP6.8319
O2	NCC NorESM2-MM	r1i1p1f1	http://doi.org/10.22033/ESGF/CMIP6.8321

Variable	Model	Variant label	DOI
pH	CMCC CMCC-ESM2	r1i1p1f1	http://doi.org/10.22033/ESGF/CMIP6.13259
pH	CNRM-CERFACS CNRM-ESM2-1	r4i1p1f2	http://doi.org/10.22033/ESGF/CMIP6.4226
pH	IPSL IPSL-CM6A-LR	r2i1p1f1	http://doi.org/10.22033/ESGF/CMIP6.5271
pH	MIROC MIROC-ES2L	r1i1p1f2	http://doi.org/10.22033/ESGF/CMIP6.5770
pH	MOHC UKESM1.0-LL	r1i1p1f2	http://doi.org/10.22033/ESGF/CMIP6.6405
pH	MRI MRI-ESM2.0	r1i2p1f1	http://doi.org/10.22033/ESGF/CMIP6.6929
pH	NCAR CESM2	r11i1p1f1	http://doi.org/10.22033/ESGF/CMIP6.7768
pH	NCAR CESM2-WACCM	r2i1p1f1	http://doi.org/10.22033/ESGF/CMIP6.10115
pH	NCC NorESM2-LM	r1i1p1f1	http://doi.org/10.22033/ESGF/CMIP6.8319
pH	NCC NorESM2-MM	r1i1p1f1	http://doi.org/10.22033/ESGF/CMIP6.8321

Table 2.9.2: Model outputs for the "sustainability" scenario (SSP1-2.6).

Variable	Model	Variant label	DOI
Thetao	BCC BCC-CSM2 MR	r1i1p1f1	http://doi.org/10.22033/ESGF/CMIP6.3028

Variable	Model	Variant label	DOI
Thetao	CAMS CAMS-CSM1.0	r1i1p1f1	http://doi.org/10.22033/ESGF/CMIP6.11046
Thetao	CCCma CanESM5	r6i1p2f1	http://doi.org/10.22033/ESGF/CMIP6.3683
Thetao	CCCma CanESM5-CanOE	r1i1p2f1	http://doi.org/10.22033/ESGF/CMIP6.10269
Thetao	CMCC CMCC-ESM2	r1i1p1f1	http://doi.org/10.22033/ESGF/CMIP6.13250
Thetao	CNRM-CERFACS CNRM-CM6-1	r3i1p1f2	http://doi.org/10.22033/ESGF/CMIP6.4184
Thetao	CNRM-CERFACS CNRM-ESM2-1	r1i1p1f2	http://doi.org/10.22033/ESGF/CMIP6.4186
Thetao	FIO-QLNM FIO-ESM 2.0	r1i1p1f1	http://doi.org/10.22033/ESGF/CMIP6.9208
Thetao	INM INM-CM4-8	r1i1p1f1	http://doi.org/10.22033/ESGF/CMIP6.12325
Thetao	INM INM-CM5-0	r1i1p1f1	http://doi.org/10.22033/ESGF/CMIP6.12326
Thetao	IPSL IPSL-CM6A-LR	r2i1p1f1	http://doi.org/10.22033/ESGF/CMIP6.5262
Thetao	MIROC MIROC6	r20i1p1f1	http://doi.org/10.22033/ESGF/CMIP6.5743
Thetao	MIROC MIROC-ES2L	r1i1p1f2	http://doi.org/10.22033/ESGF/CMIP6.5742
Thetao	MOHC HadGEM3-GC3.1-LL	r1i1p1f3	http://doi.org/10.22033/ESGF/CMIP6.10849

Variable	Model	Variant label	DOI
Thetao	MOHC UKESM1.1-LL	r1i1p1f2	http://doi.org/10.22033/ESGF/CMIP6.16841
Thetao	MOHC UKESM1.0-LL	r1i1p1f2	http://doi.org/10.22033/ESGF/CMIP6.6333
Thetao	MRI MRI-ESM2.0	r3i1p1f1	http://doi.org/10.22033/ESGF/CMIP6.6909
O2	CCCma CanESM5	r5i1p2f1	http://doi.org/10.22033/ESGF/CMIP6.3683
O2	CCCma CanESM5-CanOE	r1i1p2f1	http://doi.org/10.22033/ESGF/CMIP6.10269
O2	CMCC CMCC-ESM2	r1i1p1f1	http://doi.org/10.22033/ESGF/CMIP6.13250
O2	CNRM-CERFACS CNRM-ESM2-1	r1i1p1f2	http://doi.org/10.22033/ESGF/CMIP6.4186
O2	IPSL IPSL-CM6A-LR	r14i1p1f1	http://doi.org/10.22033/ESGF/CMIP6.5262
O2	NCAR CESM2	r4i1p1f1	http://doi.org/10.22033/ESGF/CMIP6.7746
O2	NCC NorESM2-LM	r1i1p1f1	http://doi.org/10.22033/ESGF/CMIP6.8248
O2	NCC NorESM2-MM	r1i1p1f1	http://doi.org/10.22033/ESGF/CMIP6.8250
O2	MIROC MIROC-ES2L	r1i1p1f2	http://doi.org/10.22033/ESGF/CMIP6.5742
O2	MOHC UKESM1.0-LL	r1i1p1f2	http://doi.org/10.22033/ESGF/CMIP6.6333

Variable	Model	Variant label	DOI
O2	MOHC UKESM1.1-LL	r1i1p1f2	http://doi.org/10.22033/ESGF/CMIP6.16841
pH	CMCC CMCC-ESM2	r1i1p1f1	http://doi.org/10.22033/ESGF/CMIP6.13250
pH	CNRM-CERFACS CNRM-ESM2-1	r1i1p1f2	http://doi.org/10.22033/ESGF/CMIP6.4186
pH	IPSL IPSL-CM6A-LR	r3i1p1f1	http://doi.org/10.22033/ESGF/CMIP6.5262
pH	MIROC MIROC-ES2L	r1i1p1f2	http://doi.org/10.22033/ESGF/CMIP6.5742
pH	MOHC UKESM1.0-LL	r1i1p1f2	http://doi.org/10.22033/ESGF/CMIP6.6333
pH	MOHC UKESM1.1-LL	r1i1p1f2	http://doi.org/10.22033/ESGF/CMIP6.16841
pH	NCAR CESM2	r4i1p1f1	http://doi.org/10.22033/ESGF/CMIP6.7746
pH	NCAR CESM2-WACCM	r2i1p1f1	http://doi.org/10.22033/ESGF/CMIP6.10100
pH	NCC NorESM2-LM	r1i1p1f1	http://doi.org/10.22033/ESGF/CMIP6.8248
pH	NCC NorESM2-MM	r1i1p1f1	http://doi.org/10.22033/ESGF/CMIP6.8250

Table 2.9.3: Standard deviation of climate velocities (km/yr) for the "fossil-fueled" scenario (SSP5-8.5; near future: 2015–2050), for the five focus zones (DA, JFA, RN, NCU, and SCCU).

	Temperature			Oxygen			pH		
Depth(m):	0	100	200	0	100	200	0	100	200
DA	0.61	0.4	2.15	0.42	1.11	0.27	0.75	8.68	0.95
JFA	0.63	0.93	13.79	1.03	0.78	0.32	7.08	12.51	0.93
RN	1.06	0.64	0.44	0.66	0.84	0.49	0.56	0.27	0.38
NCU	3.37	8.28	3.8	19.06	1.98	4.76	2.03	5.1	0.88
SCCU	1.57	4.26	8.23	1.18	0.16	0.8	9.14	0.84	2.77

Table 2.9.4: Percentages of climate conservation (C. %), migration (M. %), loss (L. %), and oxygenation (O. %) presented in Figure 2.4.3

	Temperature			Oxygen			pH		
Depth(m):	0	100	200	0	100	200	0	100	200
DA C. %	0	0	0	0	80	100	0	0	0
DA M. %	96.67	93.33	53.33	66.67	20	0	3.33	10	90
DA L. %	3.33	6.67	46.67	33.33	0	0	96.67	90	10
JFA C. %	0	0	0	0	83.33	100	0	0	0
JFA M. %	93.33	80	33.33	56.67	6.67	0	3.33	16.67	73.33
JFA L. %	6.67	20	66.67	43.33	10	0	96.67	83.33	26.67
RN C. %	0	0	0	0	12	0	0	0	0
RN M. %	88	92	92	76	80	96	0	0	0
RN L. %	12	8	8	24	8	4	100	100	100
NCU C. %	0	0	0	0	80.77	46.15	0	26.92	0
NCU M. %	17.95	20.51	43.59	76.92	0	0	34.62	53.85	50
NCU L. %	82.05	79.49	56.41	23.08	3.85	7.7	65.38	19.23	50
NCU O. %	0	0	0	0	15.38	46.15	0	0	0
SCCU C. %	0	7.69	0	37.5	100	93.75	0	6.25	0
SCCU M. %	53.85	30.77	16.67	50	0	0	31.25	75	87.5
SCCU L. %	46.15	61.54	83.33	12.5	0	0	68.75	18.75	12.5
SCCU O. %	0	0	0	0	0	6.25	0	0	0

Table 2.9.5: Percentages of climate conservation, migration, loss, and oxygenation/cooling presented in Figure 2.8.2.

	Temperature			Oxygen			pH		
Depth(m):	0	100	200	0	100	200	0	100	200
Conservation (%)	38.29	40.08	35.73	31.92	14.92	23.37	0	2.45	0.74
Migration (%)	41.84	40.1	37.56	43.92	61.01	46.2	20.15	23.71	22.5
Loss (%)	19.87	17.82	26.64	24.16	24.04	29.13	79.85	73.84	76.76
Oxygenation/cooling (%)	0	0	0.07	0	0.03	1.3	0	0	0

Table 2.9.6: Burrows' nine trajectories' categories, ordered (top to bottom) according to the classification steps defined by [45].

Classification	Definition	Climatic state
Non-moving	Displacement is less than 20 km in the total period (36 years in our case).	Conservation
Slow-moving	Displacement is less than 100 km, but more than 20 km in the total period (36 years in our case).	Conservation
Coastal sink	Trajectories either hit the earth or there are no nearby cells to go to.	Loss
Internal sink	Based on trajectory velocity angles, are zones in which the spatial gradient of neighboring cells converges toward their central point of intersection.	Loss
Source	When no trajectories ended in a cell (%Nend = 0).	Loss
Relative sink	When the relative number of trajectories ending in a cell was high and the proportion of starting trajectories was low (%Nend >45 %, %Nst <15 %).	Loss
Corridor	High proportion of trajectories passing through (%NFT >70 %, %Nend >0).	Loss
Divergence	Cells where fewer trajectories ended than started in that cell (%Nend <50 %, %Nst >50 %).	Migration
Convergence	Cells where more trajectories ended than started in that cell (%Nend >50 %, %Nst <50 %).	Migration

Capítulo 3

3.1. Discusión general

En esta sección se destacan los elementos más relevantes de la discusión presentada en el Capítulo 2, con el objetivo de profundizar en los hallazgos más significativos.

3.1.1. Velocidades y estados climáticos en el SEP

Para un futuro cercano, considerando un desarrollo basado en el uso de combustibles fósiles (Fossil-fueled scenario, periodo 2015–2050, Figura 2.4.1), las mayores velocidades de calentamiento se encuentran en el Sector Ecuatorial (10°S a 10°N, Figura 2.3.1) siguiendo un patrón similar a El Niño [58-60], en todas las profundidades (Figuras 2.4.1(a), (b) y (c)). Bajo la superficie (100 y 200 m), las mayores velocidades de calentamiento se extienden al HCLME (Figuras 2.4.1(b) y (c)), patrón concordante con trabajos previos, tanto para el mismo periodo [20] como para periodos previos (2000 a 2019, [47]). Lo anterior puede ser el resultado de la falta de mecanismos de enfriamiento (como la surgencia costera), que no influye a mayores profundidades [47, 61, 62]. En términos de conservación, tres refugios climáticos de temperatura yacen en el SEP, de los cuales dos se localizan en la subsuperficie tropical (5°S a 100 m, 10°S a 200 m), a pesar de la documentada expansión térmica en la zona [63-65]. El otro es un refugio constante desde la superficie hasta los 200 m, al sur de chile (55°S, Figuras 2.4.2(a), (b) y (c)). Las velocidades climáticas de oxígeno son altamente comparables a las de temperatura en superficie, concentrando las mayores velocidades de desoxigenación en el Sector Ecuatorial, presentando pérdida climática (Figura 2.4.1(d)), resultado concordante con la alta influencia del calentamiento sobre los niveles de oxígeno en la superficie oceánica. Por el contrario, en la subsuperficie, tanto el sector ecuatorial como el HCLME presentan bajas velocidades de desoxigenación,

e incluso oxigenación, clasificando casi absolutamente como zonas de conservación climática de oxígeno (Figuras 2.4.1(e) y (f)), debido posiblemente a la diversidad de procesos que regulan los niveles de oxígeno a estas profundidades [66, 67]. Esto es consistente con [20] y [37], quien teoriza la profundización de la oxiclina, y la erosión de la ZMO como efectos que podrían ser causantes de estas tendencias. La reducción de los niveles de pH se espera en todo el SEP (Figuras 2.4.1(g), (h) y (i)), para todos los casos analizados en este trabajo, siguiendo las tendencias globales [40], las cuales son más pronunciadas en escenarios de altas emisiones (SSP5-8.5) que en escenarios de mitigación (SSP1-1.9, [41]), generando un dominio de la pérdida climática del pH. Sin embargo, el HCLME muestra las menores velocidades de reducción de pH, mostrando migración, e inclusive conservación climática del pH (0.28 % a 100 m, Tabla 2.4.2, Figuras 2.4.2(h) y (i)). Lo anterior puede deberse a la relativamente alta acidez basal del HCLME [9], lo cual puede conducir a cambios más lentos.

El pH presenta las velocidades climáticas más homogéneas entre las variables (entre 10 y 30 $\frac{km}{\text{año}}$), lo que puede deberse a la amortiguación regional de cambios en el pH oceánico, causada por el intercambio aire-mar del CO2 con la atmósfera global bien mezclada [41]. También descubrimos que las velocidades climáticas de reducción de pH son mayores en latitudes altas, lo que concuerda con las observaciones de [41]. Además, nuestros resultados revelan una distribución espacial similar entre las bajas velocidades climáticas de reducción del pH y las de oxigenación en el HCLME (Figuras 2.4.1(e), (f), (h) e (i)). Este resultado sugiere una interacción dinámica entre el calentamiento, la desoxigenación y los cambios de pH en la configuración de las condiciones oceánicas, lo que resalta la complejidad de los cambios inducidos por el cambio climático en los ecosistemas marinos. En general, el pH presenta más pérdida climática, seguido de la temperatura y el oxígeno. Verticalmente (de 0 a 200 m), las velocidades climáticas de temperatura disminuyen, y las velocidades más altas se extienden desde el Sector Ecuatorial hasta el HCLME. Por otro lado, las velocidades climáticas para el pH mantienen su magnitud, pero disminuyen cerca de la costa. Por el contrario, las zonas donde las velocidades climáticas para el oxígeno son lentas en la subsuperficie son rápidas en la superficie (Figura 2.4.1). Además, las velocidades climáticas para la temperatura muestran un desplazamiento hacia el sur, las del oxígeno hacia el norte y las del pH no muestran un patrón de desplazamiento uniforme (Figura 2.4.2).

Con respecto a las zonas de enfoque, los resultados sugieren que las zonas más

alejadas de la costa americana son mas propensas a los efectos del CC. Existe alta similitud entre las zonas de surgencia (SCCU y NCU) y los archipiélagos cercanos (AJF y AD), presentando conservación climática de oxígeno, al contrario de RN, que carece casi absolutamente de zonas de conservación. Así, las zonas menos afectadas son las zonas de surgencia, seguido de los archipiélagos cercanos, y finalmente RN, la zona más afectada (Tabla 2.4.1 y Figura 2.4.3). Considerando lo anterior, la presencia de refugios climáticos de oxígeno en subsuperficie, y la presencia de las menores velocidades de reducción de pH, el HCLME sería el sector más resistente al CC dentro del SEP, resaltando su importancia en la conservación, y la prioridad de su protección.

3.1.2. Consecuencias biológicas

Las velocidades climáticas de calentamiento, tanto en la superficie sobre la plataforma continental como en las capas subsuperficiales cerca de las dorsales, podrían afectar significativamente a la fauna marina. La temperatura es el principal factor ambiental que regula las tasas metabólicas, influyendo en la supervivencia, alimentación y crecimiento [77]. Además, afecta a la solubilidad de los gases y a la interacción del pH con la fisiología de las especies, lo que puede repercutir en la demografía de las poblaciones, la estructura de las comunidades y el aumento de la exposición a especies invasoras más tolerantes al aumento de las temperaturas [77, 78]. Las condiciones subsuperficiales de oxígeno parecen favorables para las especies pelágicas y bentónicas que residen en la OMZ debido a la conservación del clima entre 100 y 200 m. Esto podría representar un refugio climático para las especies tolerantes a la hipoxia. Sin embargo, es esencial considerar el efecto sinérgico de la tríada (calentamiento, desoxigenación y aumento de pH) sobre el metabolismo de la fauna. La pérdida o migración del estado climático de temperatura y pH podría reducir el rango de tolerancia ambiental a la hipoxia, ya que aumentaría la demanda media de oxígeno de las especies residentes [72, 77, 79, 80]. Esto podría conducir a la migración de las poblaciones hacia condiciones más favorables, como desplazamientos a mayores profundidades—un fenómeno que se ha registrado durante eventos El Niño—lo que en última instancia daría lugar a cambios en la estructura de la comunidad dentro de la OMZ [78, 81]. En las comunidades mesofóticas de RN, los resultados de las velocidades climáticas de oxígeno y temperatura son menos preocupantes en comparación con los del pH. La pérdida de hábitat debida a la creciente acidificación representa una

amenaza para los corales mesofóticos, comprometiendo potencialmente la salud de las comunidades arrecifales [82, 83]. Los corales se consideran especies formadoras de hábitats, ya que proporcionan refugio y alimento a diversos taxones de vertebrados e invertebrados [84]. La degradación y mortalidad de los corales mesofóticos ya es un problema en RN, lo que conlleva la pérdida de biodiversidad en estas comunidades [85]. Las velocidades climáticas de oxigenación subsuperficial en la OMZ (200 m) sugieren una potencial expansión del hábitat en la zona epipelágica (especies no residentes) y la profundización de la OMZ, lo que podría afectar negativamente al espacio habitable de las especies dentro de la OMZ, tanto epipelágicas como bentónicas (<200 m).

En la plataforma continental, las pesquerías de peces demersales y crustáceos están compuestas por especies que habitan la OMZ (fría, hipóxica y de bajo pH), cuyos juveniles reclutan en su núcleo ($<0.5\ \frac{ml}{L}$) [81, 86-88]. Cambios en las condiciones de oxígeno, pH y temperatura, como la profundización de la oxiclina durante eventos El Niño, alteran no sólo la composición de la comunidad sino también los patrones de reclutamiento [81, 87]. Un fenómeno similar podría esperarse en las dorsales de Nazca y JFA y la porción oriental de Salas y Gómez (isla cercana a RN), ya que las comunidades parecen estar asociadas a condiciones hipóxicas subsuperficiales [89]. Los estudios futuros deberán considerar el efecto sinérgico de la tríada sobre el metabolismo y la habitabilidad de la fauna en el SEP.

3.2. Conclusión

Nuestro estudio destaca la influencia significativa del CC en los principales estresores de los ecosistemas marinos en el océano SEP, evaluados a través de la lente única de la Velocidad Climática [5, 42, 45, 46]. Esta herramienta nos permite identificar regiones con cambios climáticos rápidos, o lentos, proporcionando información sobre posibles zonas de pérdida o refugio climático. El enfoque multi-estresor, en cuanto al análisis de tres (temperatura, oxígeno y pH) de los cuatro principales estresores sugeridos por [43], y también el enfoque multidimensional (diferentes profundidades, periodos y escenarios climáticos) permite aumentar nuestra comprensión sobre la influencia del CC. Así, identificamos zonas que han demostrado resistencia al CC y, por tanto, resaltan su gran importancia ecológica. La costa de Perú-Chile (HCLME) en la subsuperficie presenta refugios climáticos de oxígeno y las velocidades climáticas

de reducción de pH más bajas, a pesar de la pérdida climática de temperatura. El sur de Chile comprende un refugio climático de temperatura en toda la vertical analizada, así como dos zonas oceánicas tropicales en la subsuperficie, a pesar de la expansión térmica prevista. Nuestro análisis de los efectos del CC en las zonas focales sugiere una mayor resistencia al CC en las regiones cercanas a la costa. Así, la región entre los archipiélagos y los sistemas de surgencia podría ser una zona clave para la conservación de la vida marina y, por tanto, merecería una protección prioritaria. El análisis comparativo de los dos escenarios deja en manifiesto que la vía de desarrollo basada en los combustibles fósiles (SSP5-8.5) supone una gran amenaza para los entornos marinos, como demuestran las velocidades climáticas de calentamiento y reducción del pH consistentemente superiores. En cambio, este escenario parece mostrar mayores velocidades climáticas de oxigenación y menores de desoxigenación que el escenario de sostenibilidad (SSP1-2.6), pero sólo en el futuro próximo. Sin embargo, existe gran heterogeneidad entre los modelos, lo que disminuye el realismo y la fiabilidad de estos resultados de oxígeno en el escenario de sostenibilidad.

Estos resultados enfatizan la necesidad crítica de prácticas sostenibles para mitigar los impactos adversos. Este trabajo revela posibles escenarios futuros de cambios en los hábitats y los ecosistemas, constituyendo un recurso crucial para fundamentar las estrategias de conservación, las prácticas pesqueras sostenibles y la gestión de las zonas marinas protegidas. La integración de estos conocimientos nos permitirá anticiparnos y prepararnos mejor para las consecuencias ecológicas del CC y, en última instancia, contribuir a preservar y mantener la biodiversidad marina del SEP.

Bibliografía

[1] Canadell, J.G., P.M.S. Monteiro, M.H. Costa, L. Cotrim da Cunha, P.M. Cox, A.V. Eliseev, S. Henson, M. Ishii, S. Jaccard, C. Koven, A. Lohila, P.K. Patra, S. Piao, J. Rogelj, S. Syampungani, S. Zaehle, and K. Zickfeld, 2021: Global Carbon and other Biogeochemical Cycles and Feedbacks. In Climate Change 2021: The Physical Science Basis. Contribution of Working Group I to the Sixth Assessment Report of the Intergovernmental Panel on Climate Change [Masson-Delmotte, V., P. Zhai, A. Pirani, S.L. Connors, C. Péan, S. Berger, N. Caud, Y. Chen, L. Goldfarb, M.I. Gomis, M. Huang, K. Leitzell, E. Lonnoy, J.B.R. Matthews, T.K. Maycock, T. Waterfield, O. Yelekçi, R. Yu, and B. Zhou (eds.)]. Cambridge University Press, Cambridge, United Kingdom and New York, NY, USA, pp. 673–816, doi:10.1017/9781009157896.007.

[2] Liu, Z., Deng, Z., Davis, S., & Ciais, P. (2023). Monitoring global carbon emissions in 2022. Nature Reviews Earth & Environment, 4(4), 205-206. https://doi.org/10.1038/s43017-023-00406-z.

[3] IPCC, 2023: Summary for Policymakers. In: Climate Change 2023: Synthesis Report. Contribution of Working Groups I, II and III to the Sixth Assessment Report of the Intergovernmental Panel on Climate Change [Core Writing Team, H. Lee and J. Romero (eds.)]. IPCC, Geneva, Switzerland, pp. 1-34, doi: 10.59327/IPCC/AR6-9789291691647.001.

[4] Thomas, C. D., Cameron, A., Green, R. E., Bakkenes, M., Beaumont, L. J., Collingham, Y. C., Erasmus, B. F. N., De Siqueira, M. F., Grainger, A., Hannah, L., Hughes, L., Huntley, B., Van Jaarsveld, A. S., Midgley, G. F., Miles, L., Ortega-Huerta, M. A., Peterson, A. T., Phillips, O. L. & Williams, S. E. (2004). Extinction risk from climate change. Nature, 427(6970), 145-148. https://doi.org/10.1038/nature02121.

[5] Brito-Morales, I., Molinos, J. G., Schoeman, D. S., Burrows, M. T., Poloczanska, E. S., Brown, C. J., Ferrier, S., Harwood, T. D., Klein, C. J., McDonald-Madden, E., Moore, P. J., Pandolfi, J. M., Watson, J. E. M., Wenger, A. S., & Richardson, A. J. (2018). Climate velocity can inform conservation in a warming world. Trends in ecology & evolution, 33(6), 441-457. https://doi.org/10.1016/j.tree.2018.03.009.

[6] Neelmani, R. C., Pal, M., Sarman, V., Vyas, U. D., & Muniya, T. N. (2019). Impacts of climate change on marine biodiversity. Journal of Entomology and Zoology Studies, 7(2), 425-430.

[7] Feely, R. A., Doney, S. C., & Cooley, S. R. (2009). Ocean acidification: Present conditions and future changes in a high-CO_2 world. Oceanography, 22(4), 36-47.

[8] Henson, S. A., Beaulieu, C., & Lampitt, R. (2016). Observing climate change trends in ocean biogeochemistry: when and where. Global change biology, 22(4), 1561-1571.

[9] Gutiérrez, D., Akester, M., & Naranjo, L. (2016). Productivity and sustainable management of the Humboldt current large marine ecosystem under climate change. Environmental Development, 17, 126-144.

[10] Oschlies, A. (2021). A committed fourfold increase in ocean oxygen loss. Nature Communications, 12(1), 2307.

[11] Pequeño, G., & Sáez, S. (2000). Los peces litorales del archipiélago de Juan Fernández (Chile): endemismo y relaciones ictiogeográficas. Investigaciones marinas, 28, 27-37.

[12] Friedlander, A. M., Ballesteros, E., Beets, J., Berkenpas, E., Gaymer, C. F., Gorny, M., & Sala, E. (2013). Effects of isolation and fishing on the marine ecosystems of Easter Island and Salas y Gómez, Chile. Aquatic Conservation: Marine and Freshwater Ecosystems, 23(4), 515-531.

[13] Friedlander, A. M., Ballesteros, E., Caselle, J. E., Gaymer, C. F., Palma, A. T., Petit, I., Varas, E., Wilson, A. M., & Sala, E. (2016). Marine biodiversity in Juan Fernández and Desventuradas Islands, Chile: global endemism hotspots. PLoS One, 11(1), e0145059.

[14] Petit, I. J., Campoy, A. N., Hevia, M. J., Gaymer, C. F., & Squeo, F. A. (2018). Protected areas in Chile: are we managing them?. Revista chilena de historia natural, 91.

[15] Pauly, D., & Christensen, V. (1995). Primary production required to sustain global fisheries. Nature, 374(6519), 255-257.

[16] Heileman, S., Guevara, R., Chavez, F., Bertrand, A., and Soldi, H. (2009). "XVII-56 humboldt current?: LME # 13," in The UNEP LargeMarine Ecosystem Report: A Perspective on Changing Conditions in LMEs of the World's Regional Seas, eds K. Sherman and G. Hempel (Nairobi: United Nations Environment Programme).

[17] Parada, C., Gretchina, A., Vásquez, S., Belmadani, A., Combes, V., Ernst, B., Di Lorenzo, E., Porobic J. & Sepúlveda, A. (2017). Expanding the conceptual framework of the spatial population structure and life history of jack mackerel in the eastern South Pacific: an oceanic seamount region as potential spawning/nursery habitat. ICES Journal of Marine Science, 74(9), 2398-2414.

[18] Paredes, F., Flores, D., Figueroa, A., Gaymer, C. F., & Aburto, J. A. (2019). Science, capacity building and conservation knowledge: the empowerment of the local community for marine conservation in Rapa Nui. Aquatic Conservation: Marine and Freshwater Ecosystems, 29, 130-137.

[19] Porobic, J., Fulton, E. A., Parada, C., Frusher, S., Ernst, B., & Manríquez, P. (2019). The impact of fishing on a highly vulnerable ecosystem, the case of Juan Fernández Ridge ecosystem. Plos one, 14(2), e0212485.

[20] Dewitte, B., Conejero, C., Ramos, M., Bravo, L., Garcon, V., Parada, C., Sellanes, J., Mecho, A., Muñoz, P., & Gaymer, C. F. (2021). Understanding the impact of climate change on the oceanic circulation in the Chilean island ecoregions. Aquatic Conservation: Marine and Freshwater Ecosystems, 31(2), 232-252.

[21] Porobic, J., Parada, C., Ernst, B., Hormazábal, S. E., & Combes, V. (2012). Modelación de la conectividad de las subpoblaciones de la langosta de Juan Fernández (Jasus frontalis), a través de un modelo biofísico. Latin american journal of aquatic research, 40(SPECISSUE), 613-632.

[22] Cornejo-Guzmán, S. (2018). Mecanismos de mesoescala y variables biogeoquímicas que determinan la variabilidad de clorofila-a en el Archipiélago de Juan Fernández (undergraduate thesis). Universidad de Concepción, Chile.

[23] Gennip, S.J.V., Dewitte, B., Garçon, V. et al. In search for the sources of plastic marine litter that contaminates the Easter Island Ecoregion. Sci Rep 9, 19662 (2019). https://doi.org/10.1038/s41598-019-56012-x.

[24] Guinotte, J. M., & Fabry, V. J. (2008). Ocean acidification and its potential effects on marine ecosystems. Annals of the New York Academy of Sciences, 1134(1), 320-342.

[25] Sunday, J. M., Bates, A. E., & Dulvy, N. K. (2012). Thermal tolerance and the global redistribution of animals. Nature Climate Change, 2(9), 686-690.

[26] Parouffe, A., Garçon, V., Dewitte, B., Paulmier, A., Montes, I., Parada, C., Mecho, A., & Veliz, D. (2023). Evaluating future climate change exposure of marine habitat in the South East Pacific based on metabolic constraints. Frontiers in Marine Science, 9, 1055875.

[27] Lehner, F., Deser, C., Maher, N., Marotzke, J., Fischer, E. M., Brunner, L., Knutti, R., & Hawkins, E. (2020). Partitioning climate projection uncertainty with multiple large ensembles and CMIP5/6. Earth System Dynamics, 11(2), 491-508.

[28] Vecchi, G. A., Soden, B. J., Wittenberg, A. T., Held, I. M., Leetmaa, A., & Harrison, M. J. (2006). Weakening of tropical Pacific atmospheric circulation due to anthropogenic forcing. Nature, 441(7089), 73-76.

[29] DiNezio, P. N., Clement, A. C., Vecchi, G. A., Soden, B. J., Kirtman, B. P., & Lee, S. K. (2009). Climate response of the equatorial Pacific to global warming. Journal of Climate, 22(18), 4873-4892.

[30] Liu, Z., Vavrus, S., He, F., Wen, N., & Zhong, Y. (2005). Rethinking tropical ocean response to global warming: The enhanced equatorial warming. Journal of Climate, 18(22), 4684-4700.

[31] Timmermann, A., McGregor, S., & Jin, F. F. (2010). Wind effects on past and future regional sea level trends in the southern Indo-Pacific. Journal of Climate, 23(16), 4429-4437.

[32] Lu, J., Vecchi, G. A., & Reichler, T. (2007). Expansion of the Hadley cell under global warming. Geophysical Research Letters, 34(6).

[33] Xie, S. P., Deser, C., Vecchi, G. A., Ma, J., Teng, H., & Wittenberg, A. T. (2010). Global warming pattern formation: Sea surface temperature and rainfall. Journal of Climate, 23(4), 966-986.

[34] Thual. S., B. Dewitte, S.-I. An, S. Illig and N. Ayoub, 2013: Influence of Recent Stratification Changes on ENSO stability in a Conceptual Model of the Equatorial Pacific. J. Climate, 26, 4790-4802. https://doi.org/10.1175/JCLI-D-12-00363.1.

[35] Schmidtko, S., Stramma, L., & Visbeck, M. (2017). Decline in global oceanic oxygen content during the past five decades. Nature, 542(7641), 335-339.

[36] Breitburg, D., Levin, L. A., Oschlies, A., Grégoire, M., Chavez, F. P., Conley, D. J., Garçon, V., Gilbert, D., Gutiérrez, D., Isensee, K., Jacinto, G. S., Limburg, K. E., Montes, I., Naqvi, S. W. A., Pitcher, G. C., Rabalais, N. N., Roman, M. R., Rose, K. A., Seibel, B. A., Telszewski, M., Yasuhara, M., & Zhang, J. (2018). Declining oxygen in the global ocean and coastal waters. Science, 359(6371), eaam7240.

[37] Almendra, I., Dewitte, B., Garçon, V., Muñoz, P., Parada, C., Montes, I., Paulmier, A., & Oschlies, A. (2024). Emergent constraint on oxygenation of the upper South Eastern Pacific oxygen minimum zone in the twenty-first century. Communications Earth & Environment, 5(1), 284.

[38] Gallardo, M. A., Rojas, I., Brokordt, K., Lovrich, G., Nuñez, V., Paschke, K., Carrasco, F. D., & Yannicelli, B. (2019). Life on the edge: incubation behaviour and physiological performance of squat lobsters in oxygen-minimum conditions. Marine Ecology Progress Series, 623, 51-70.

[39] Doney, S. C., Fabry, V. J., Feely, R. A., & Kleypas, J. A. (2009). Ocean acidification: the other CO2 problem. Annual review of marine science, 1, 169-192.

[40] Iida, Y., Takatani, Y., Kojima, A., & Ishii, M. (2021). Global trends of ocean CO 2 sink and ocean acidification: an observation-based reconstruction of surface ocean inorganic carbon variables. Journal of Oceanography, 77, 323-358.

[41] Jiang, L. Q., Dunne, J., Carter, B. R., Tjiputra, J. F., Terhaar, J., Sharp, J. D., Ilyina, T., & Ziehn, T. (2023). Global surface ocean acidification indicators from 1750 to 2100. Journal of Advances in Modeling Earth Systems, 15(3), e2022MS003563.

[42] Loarie, S. R., Duffy, P. B., Hamilton, H., Asner, G. P., Field, C. B., & Ackerly, D. D. (2009). The velocity of climate change. Nature, 462(7276), 1052-1055.

[43] Bopp, L., Resplandy, L., Orr, J. C., Doney, S. C., Dunne, J. P., Gehlen, M., Halloran, P., Heinze, C., Ilyina, T., Séférian, R., Tjiputra, J., & Vichi, M. (2013). Multiple stressors of ocean ecosystems in the 21st century: projections with CMIP5 models. Biogeosciences, 10(10), 6225-6245.

[44] Burrows, M. T., Schoeman, D. S., Buckley, L. B., Moore, P., Poloczanska, E. S., Brander, K. M., Brown, C., Bruno, J. F., Duarte, C. M., Halpern, B. S., Holding, J., Kappel, C. V., Kiessling, W., O'Connor, M. I., Pandolfi, J. M., Parmesan, C.,

Schwing, F. B., Sydeman, W. J., & Richardson, A. J. (2011). The pace of shifting climate in marine and terrestrial ecosystems. Science, 334(6056), 652-655.

[45] Burrows, M. T., Schoeman, D. S., Richardson, A. J., Molinos, J. G., Hoffmann, A., Buckley, L. B., Moore, P. J., Brown, C. J., Bruno, F. J., Duarte, C. M., Halpern, B. S., Hoegh-Guldberg, O., Kappel, C. V., Kiessling, W., O'Connor, M., Pandolfi, J. M., Parmesan, C., Sydeman, W. J., Ferrier, S., Williams, K. J., & Poloczanska, E. S. (2014). Geographical limits to species-range shifts are suggested by climate velocity. Nature, 507(7493), 492-495.

[46] García Molinos, J., Schoeman, D. S., Brown, C. J., & Burrows, M. T. (2019). VoCC: An r package for calculating the velocity of climate change and related climatic metrics. Methods in Ecology and Evolution, 10(12), 2195-2202.

[47] de la Maza, L., Wieters, E. A., Beldade, R., Landaeta, M. F., Perez-Matus, A., & Navarrete, S. A. (2024). Variability in oceanographic conditions affecting Mesophotic Ecosystems along the South Eastern Pacific: Latitudinal trends and potential for climate refugia. Journal of Marine Systems, 245, 103999.

[48] Morelli, T. L., Daly, C., Dobrowski, S. Z., Dulen, D. M., Ebersole, J. L., Jackson, S. T., Lundquist, J. D., Millar, C. I., & Beissinger, S. R. (2016). Managing climate change refugia for climate adaptation. PloS one, 11(8), e0159909. [49] Keppel, G., & Wardell-Johnson, G. W. (2012). Refugia: keys to climate change management. Global change biology, 18(8), 2389-2391.

[50] Keppel, G., Mokany, K., Wardell-Johnson, G. W., Phillips, B. L., Welbergen, J. A., & Reside, A. E. (2015). The capacity of refugia for conservation planning under climate change. Frontiers in Ecology and the Environment, 13(2), 106-112.

[51] Kavousi, J., & Keppel, G. (2018). Clarifying the concept of climate change refugia for coral reefs. ICES Journal of Marine Science, 75(1), 43-49.

[52] Arafeh-Dalmau, N., Brito-Morales, I., Schoeman, D. S., Possingham, H. P., Klein, C. J., & Richardson, A. J. (2021). Incorporating climate velocity into the design of climate-smart networks of marine protected areas. Methods in Ecology and Evolution, 12(10), 1969-1983.

[53] Eyring, V., Bony, S., Meehl, G. A., Senior, C. A., Stevens, B., Stouffer, R. J., & Taylor, K. E. (2016). Overview of the Coupled Model Intercomparison Project Phase 6 (CMIP6) experimental design and organization. Geoscientific Model Development, 9(5), 1937-1958.

[54] O'Neill, B. C., Tebaldi, C., Van Vuuren, D. P., Eyring, V., Friedlingstein, P., Hurtt, G., Knutti, R., Kriegler, E., Lamarque, J., Lowe, J., Meehl, G. A., Moss, R., Riahi, K., & Sanderson, B. M. (2016). The scenario model intercomparison project (ScenarioMIP) for CMIP6. Geoscientific Model Development, 9(9), 3461-3482.

[55] Montecinos, A., & Gomez, F. (2010). ENSO modulation of the upwelling season off southern-central Chile. Geophysical Research Letters, 37(2).

[56] R Core Team (2021). R: A language and environment for statistical computing. R Foundation for Statistical Computing, Vienna, Austria. URL https://www.R-project.org/.

[57] Singh, K., & Xie, M. (2008). Bootstrap: a statistical method. Unpublished manuscript, Rutgers University, USA. Retrieved from http://www. stat. rutgers. edu/home/mxie/RCPapers/bootstrap. pdf, 1-14.

[58] Meehl, G. A., & Washington, W. M. (1996). El Niño-like climate change in a model with increased atmospheric CO2 concentrations. Nature, 382(6586), 56-60.

[59] Collins, M. (2005). El Niño-or La Niña-like climate change?. Climate Dynamics, 24, 89-104.

[60] Lian, T., Chen, D., Ying, J., Huang, P., & Tang, Y. (2018). Tropical Pacific trends under global warming: El Niño-like or La Niña-like?. National Science Review, 5(6), 810-812.

[61] Winckler Grez, P., Aguirre, C., Farías, L., Contreras-López, M., & Masotti, Í. (2020). Evidence of climate-driven changes on atmospheric, hydrological, and oceanographic variables along the Chilean coastal zone. Climatic Change, 163(2), 633-652.

[62] Aguirre, C., Flores-Aqueveque, V., Vilches, P., Vásquez, A., Rutllant, J. A., & Garreaud, R. (2021). Recent changes in the low-level jet along the subtropical west coast of South America. Atmosphere, 12(4), 465.

[63] Seidel, D. J., Fu, Q., Randel, W. J., & Reichler, T. J. (2008). Widening of the tropical belt in a changing climate. Nature geoscience, 1(1), 21-24.

[64] Vergés, A., Steinberg, P. D., Hay, M. E., Poore, A. G., Campbell, A. H.,

Ballesteros, E., Heck, K. L., Booth, D. J., & Wilson, S. K. (2014). The tropicalization of temperate marine ecosystems: climate-mediated changes in herbivory and community phase shifts. Proceedings of the Royal Society B: Biological Sciences, 281(1789), 20140846.

[65] Staten, P. W., Lu, J., Grise, K. M., Davis, S. M., & Birner, T. (2018). Re-examining tropical expansion. Nature Climate Change, 8(9), 768-775.Stramma, L., Johnson, G. C., Sprintall, J., & Mohrholz, V. (2008). Expanding oxygen-minimum zones in the tropical oceans. science, 320(5876), 655-658.

[66] Karstensen, J., Stramma, L., & Visbeck, M. (2008). Oxygen minimum zones in the eastern tropical Atlantic and Pacific oceans. Progress in Oceanography, 77(4), 331-350.

[67] Llanillo, P. J., Pelegrí, J. L., Talley, L. D., Peña-Izquierdo, J., & Cordero, R. R. (2018). Oxygen pathways and budget for the eastern South Pacific oxygen minimum zone. Journal of Geophysical Research: Oceans, 123(3), 1722-1744.

[68] Pinsky, M. L., Worm, B., Fogarty, M. J., Sarmiento, J. L., & Levin, S. A. (2013). Marine taxa track local climate velocities. Science, 341(6151), 1239-1242.

[69] Louthan, A. M., DeMarche, M. L., & Shoemaker, L. G. (2021). Climate sensitivity across latitude: scaling physiology to communities. Trends in Ecology & Evolution, 36(10), 931-942.

[70] Bernatchez, L., Ferchaud, A. L., Berger, C. S., Venney, C. J., & Xuereb, A. (2024). Genomics for monitoring and understanding species responses to global climate change. Nature Reviews Genetics, 25(3), 165-183.

[71] Osores, S. J., Lagos, N. A., San Martin, V., Manriquez, P. H., Vargas, C. A., Torres, R., Navarro, J. M., Poupin, M. J., Saldías G. S., & Lardies, M. A. (2017). Plasticity and inter-population variability in physiological and life-history traits of the mussel Mytilus chilensis: a reciprocal transplant experiment. Journal of Experimental Marine Biology and Ecology, 490, 1-12.

[72] Deutsch, C., Penn, J. L., & Seibel, B. (2020). Metabolic trait diversity shapes marine biogeography. Nature, 585(7826), 557-562. https://doi.org/10.1038/s41586-020-2721-y.

[73] Zheng, Y., Shinoda, T., Lin, J. L., & Kiladis, G. N. (2011). Sea surface temperature biases under the stratus cloud deck in the southeast Pacific Ocean in 19

IPCC AR4 coupled general circulation models. Journal of Climate, 24(15), 4139-4164.

[74] Hourdin, F., Găinusă-Bogdan, A., Braconnot, P., Dufresne, J. L., Traore, A. K., & Rio, C. (2015). Air moisture control on ocean surface temperature, hidden key to the warm bias enigma. Geophysical Research Letters, 42(24), 10-885.

[75] Exarchou, E., Prodhomme, C., Brodeau, L., Guemas, V., & Doblas-Reyes, F. (2018). Origin of the warm eastern tropical Atlantic SST bias in a climate model. Climate Dynamics, 51, 1819-1840.

[76] Zhang, Q., Liu, B., Li, S., & Zhou, T. (2023). Understanding models' global sea surface temperature bias in mean state: from CMIP5 to CMIP6. Geophysical Research Letters, 50(4), e2022GL100888.

[77] Pörtner, H.-O. (2010). Oxygen- and capacity-limitation of thermal tolerance: A matrix for integrating climate-related stressor effects in marine ecosystems. Journal of Experimental Biology, 213(6), 881-893. https://doi.org/10.1242/jeb.037523.

[78] Clarke, T. M., Frölicher, T., Reygondeau, G., Villalobos-Rojas, F., Wabnitz, C. C. C., Wehrtmann, I. S., & Cheung, W. W. L. (2022). Temperature and oxygen supply shape the demersal community in a tropical Oxygen Minimum Zone. Environmental Biology of Fishes, 105(10), 1317-1333. https://doi.org/10.1007/s10641-022-01256-2.

[79] Pörtner, H. O., & Farrell, A. P. (2008). Physiology and Climate Change. Science, 322(5902), 690-692. https://doi.org/10.1126/science.1163156.

[80] Pörtner, H. (2012). Integrating climate-related stressor effects on marine organisms: Unifying principles linking molecule to ecosystem-level changes. Marine Ecology Progress Series, 470, 273-290. https://doi.org/10.3354/meps10123.

[81] Quiroga, E., Sellanes, J., Arntz, W. E., Gerdes, D., Gallardo, V. A., & Hebbeln, D. (2009). Benthic megafaunal and demersal fish assemblages on the Chilean continental margin: The influence of the oxygen minimum zone on bathymetric distribution. Deep Sea Research Part II: Topical Studies in Oceanography, 56(16), 1112-1123. https://doi.org/10.1016/j.dsr2.2008.09.010.

[82] Rossi, S., Bramanti, L., Gori, A., & Orejas, C. (Eds.). (2017). Marine Animal Forests: The Ecology of Benthic Biodiversity Hotspots. Springer International Publishing. https://doi.org/10.1007/978-3-319-21012-4.

[83] Talukder, B., Ganguli, N., Matthew, R., vanLoon, G. W., Hipel, K. W., & Orbinski, J. (2022). Climate change-accelerated ocean biodiversity loss & associated planetary health impacts. The Journal of Climate Change and Health, 6, 100114. https://doi.org/10.1016/j.joclim.2022.100114.

[84] Samadi, S., Schlacher, T., & De Forges, B. R. (2007). Seamount Benthos. En T. J. Pitcher, T. Morato, P. J. B. Hart, M. R. Clark, N. Haggan, & R. S. Santos (Eds.), Seamounts: Ecology, Fisheries & Conservation (pp. 117-140). Blackwell Publishing Ltd. https://doi.org/10.1002/9780470691953.ch7.

[85] Basualto, V. (2024). Estresores oceanográficos y antropogénicos en corales someros de rapa Nui: Una reconstrucción paleoambiental del impacto del siglo XXI [Undergrade Thesis]. Departamento de Biología Marina. Universidad Católica del Norte.

[86] Gallardo, V. A., Canete, J. I., Enriquez-Briones, S., & Baltazar, M. (1994). Recruitment of the squat lobster Pleuroncodes monodon on the continental shelf off Central Chile. Journal or Crustacean Biology, 14(4), 665-669.

[87] Gallardo, V. A., Palma, M., Carrasco, F. D., Gutiérrez, D., Levin, L. A., & Cañete, J. I. (2004). Macrobenthic zonation caused by the oxygen minimum zone on the shelf and slope off central Chile. Deep Sea Research Part II: Topical Studies in Oceanography, 51(20-21), 2475-2490. https://doi.org/10.1016/j.dsr2.2004.07.028.

[88] Gallardo, M.A., González López, A. E., Ramos, M., Mujica, A., Muñoz, P., Sellanes, J., & Yannicelli, B. (2017). Reproductive patterns in demersal crustaceans from the upper boundary of the OMZ off north-central Chile. Continental Shelf Research, 141, 26-37. https://doi.org/10.1016/j.csr.2017.04.011.

[89] Fernández-Zúñiga, M., Vögler, R., Gallardo, M. A., Tapia-Guerra, J. M., & Sellanes, J. (in review). Spatial ecology of two emblematic crustacean in deep-sea ecosystems at Salas & Gómez, Nazca and Juan Fernández ridges (Southeast Pacific). Scientific Reports.

[90] Riahi, K., Van Vuuren, D. P., Kriegler, E., Edmonds, J., O'neill, B. C., Fujimori, S., Bauer, N., Calvin, K., Dellink, R., Fricko, O., Lutz, W., Popp, A., Cuaresma, J. C., Samir, K. C., Leimbach, M., Jiang, L., Kram, T., Rao, S., Emmerling, J., Ebi, K., Hasegawa, T., Havlik, P., Humpenöder, F., Da silva, L. A., Smith, S., Stehfest, E., Bosetti, V., Eom, J., Gernaat, D., Masui, T., Rogelj, J., Strefler, J., Drouet, L., Krey, V., Luderer, G., Harmsen, M., Takahashi, K., Baumstark, L., Doelman, J. C., Kainuma, M., Klimont, Z., Marangoni, G., Lotze-Campen, H., Obersteiner, M., Tabeau, A., & Tavoni, M. (2017). The Shared Socioeconomic Pathways and their

energy, land use, and greenhouse gas emissions implications: An overview. Global environmental change, 42, 153-168.

[91] O'Neill, B. C., Tebaldi, C., Van Vuuren, D. P., Eyring, V., Friedlingstein, P., Hurtt, G., Knutti, R., Kriegler, E., Lamarque, J., Lowe, J., Meehl, G. A., Moss, R., Riahi, K., & Sanderson, B. M. (2016). The scenario model intercomparison project (ScenarioMIP) for CMIP6. Geoscientific Model Development, 9(9), 3461-3482.

[92] Moss, R. H., Edmonds, J. A., Hibbard, K. A., Manning, M. R., Rose, S. K., Van Vuuren, D. P., Carter, T. R., Emori, S., Kainuma, M., Kram T., Meehl, G. A., Mitchel, J. F. B., Nakicenovic, N., Riahi K., Smith, S. J., Stouffer, R. J., Thomson, A. M., Weyant, J. P., & Wilbanks, T. J. (2010). The next generation of scenarios for climate change research and assessment. Nature, 463(7282), 747-756.